DOI:
10.1183/13993003.02171-2023

Document Version
Peer reviewed version

EUROPEAN RESPIRATORY *journal*

FLAGSHIP SCIENTIFIC JOURNAL OF ERS

Early View

Original Research Article

CD94+ Natural Killer cells potentiate pulmonary ischemia-reperfusion injury

Tasha Tsao, Longhui Qiu, Reena Bharti, Avishai Shemesh, Alberto M. Hernandez, Simon J. Cleary, Nancy Y. Greenland, Jesse Santos, Ruoshi Shi, Lu Bai, Jennifer Richardson, Kimberley Dilley, Matthias Will, Nenad Tomasevic, Tereza Sputova, Adam Salles, Jeffrey Kang, Dongliang Zhang, Steve R. Hays, Jasleen Kukreja, Jonathan P. Singer, Lewis L. Lanier, Mark R. Looney, John R. Greenland, Daniel R. Calabrese

Please cite this article as: Tsao T, Qiu L, Bharti R, *et al*. CD94+ Natural Killer cells potentiate pulmonary ischemia-reperfusion injury. *Eur Respir J* 2024; in press (https://doi.org/10.1183/13993003.02171-2023).

CD94+ Natural Killer cells potentiate pulmonary ischemia-reperfusion injury

Authors: Tasha Tsao[1,†], Longhui Qiu[1,†], Reena Bharti[1], Avishai Shemesh[1,2],Alberto M. Hernandez[2,3], Simon J. Cleary[4], Nancy Y. Greenland[5], Jesse Santos[6], Ruoshi Shi[7], Lu Bai[7], Jennifer Richardson[7], Kimberley Dilley[7], Matthias Will[7], Nenad Tomasevic[7], Tereza Sputova[7], Adam Salles[7], Jeffrey Kang[7], Dongliang Zhang[1], Steve R. Hays[1], Jasleen Kukreja[8], Jonathan P. Singer[1], Lewis L. Lanier[2,3], Mark R. Looney[1], John R. Greenland[1,9], Daniel R. Calabrese[1,9*]

ORCIDS: DRC 0000-0002-0596-3434, JPS 0000-0003-0224-7472, MRL 0000-0003-0241-9190,
JRG 0000-0003-1422-8367, SJC 0000-0001-5573-6363

Affiliations:
[1]*Department of Medicine, University of California, San Francisco, CA*
[2]*Parker Institute for Cancer Immunotherapy San Francisco, CA*
[3]*Department of Microbiology and Immunology, University of California, San Francisco, CA*
[4]*Institute of Pharmaceutical Science, King's College London, UK*
[5]*Department of Pathology, University of California, San Francisco, CA*
[6]*Department of Surgery, University of California San Francisco - East Bay, Oakland, CA*
[7]*Dren Bio, Foster City, CA*
[8]*Departmentof Surgery, University of California, San Francisco, CA.*
[9]*Medical Service, Veterans Affairs Health Care System, San Francisco, CA.*
[†]*These authors contributed equally.*
**Corresponding author*

Correspondence and reprint requests:
Dr. Daniel R. Calabrese
San Francisco VA Medical Center
4150 Clement St
San Francisco, CA 94121, USA
415-221-4810

List of non-standard abbreviations:
APC, antigen-presenting cell
CMV, cytomegalovirus
IRI, ischemia-reperfusion injury
NK, Natural killer
PBMC, peripheral blood mononuclear cell
PGD, primary graft dysfunction
RC, receptor complex

ABSTRACT

Pulmonary ischemia-reperfusion injury (IRI) is a major contributor to poor lung transplant outcomes. We recently demonstrated a central role of airway-centered NK cells in mediating IRI; however, there are no existing effective therapies for directly targeting NK cells in humans. We hypothesized that a depleting anti-CD94 monoclonal antibody (mAb) would provide therapeutic benefit in mouse and human models of IRI based on high levels of *KLRD1* (CD94) transcripts in bronchoalveolar lavage samples from lung transplant patients. We found that CD94 is highly expressed on mouse and human NK cells, with increased expression during IRI. Anti-mouse and anti-human mAbs against CD94 showed effective NK cell depletion in mouse and human models and blunted lung damage and airway epithelial killing. In two different allogeneic orthotopic lung transplant mouse models, anti-CD94 treatment during induction reduced early lung injury and chronic inflammation relative to control therapies. Anti-CD94 did not increase donor antigen-presenting cells that could alter long-term graft acceptance. Lung transplant induction regimens incorporating anti-CD94 treatment may safely improve early clinical outcomes.

INTRODUCTION

Lung transplantation is a life-prolonging therapy for patients with advanced lung disease [1]. However, the potential benefit of lung transplant is hampered by early ischemia reperfusion injury (IRI) [2]. Severe IRI manifests clinically as primary graft dysfunction (PGD), defined as diffuse bilateral pulmonary opacities on imaging and hypoxemia during day 2 or 3 following transplantation [3]. PGD is a multifaceted disease that occurs in up to 1/3 of all lung transplant recipients, drives 50% of the first-year mortality, is associated with poor quality of life and chronic rejection, and is increasing in incidence [4-8]. Like other acute lung injury syndromes, PGD has no medical therapies known to be effective for prevention or improvement of injury.

The pathophysiology of IRI results from a cascade of events initiated with endothelial and epithelial injury leading to inflammatory mediator release and graft infiltration by innate immune cells [9]. We have described a central role for Natural Killer (NK) cells in mediating the early injury of IRI [10]. NK cells are innate immune cells with the primary function to surveil for missing, damaged, or transformed self [11]. In contrast to B and T cells, where antigen specificity is dependent upon genetic rearrangement, NK cell actions are determined by the integration of a myriad of somatically encoded inhibitory or activating receptors [10]. In experimental models of IRI and in human PGD samples, we identified that NK cell activation occurs via recognition of stress molecules on the surfaces of epithelial and endothelial cells through the NKG2D receptor [12-14]. Moreover, NK cell depletion or NKG2D blockade blunted lung injury *in vitro* and *in vivo*.

Lung transplant recipients can receive a variety of immunosuppression agents throughout the life of the allograft [15]. Pertinent to PGD, many centers give induction regimens that contain corticosteroids, anti-thymocyte globulin, calcineurin inhibitors, cell cycle inhibitors, or IL-2 receptor blockade [16]. Notably, NK cells are resistant to many of these agents as they are resident in the graft and thus difficult to expose to therapeutic drug concentrations. Moreover, their effector functions are not dependent upon transcription as they store their effector molecules in pre-formed cytoplasmic granules [17]. In fact, IL-2 receptor blockade may lead to NK cell activation through secondary scavenging of IL-2 [18]. mTOR inhibition dampens NK cell function but cannot be given early after lung transplant due to issues with anastomotic healing [19, 20]. To date, there are no NK cell specific therapies available for direct depletion or broad receptor inhibition in humans.

Mouse and human NK cells have many homologous receptors, co-receptors, and adapter molecules [21]. While NK cell depletion targeting the NK1.1 receptor results in efficient depletion of mouse NK cells, there has not yet been a successful approach in effecting human NK cell depletion and the human ortholog of NK1.1 (CD161) is not expressed by all NK cells [13, 22]. Moreover, targeting NK cells via NKG2D receptor blockade in inflammatory bowel disease did not result in clinically meaningful differences in outcomes in most patients [23].

Thus, there is need for an alternate and broader NK cell targeted approach. Here, we sought to identify a novel target for NK cell subset depletion. We hypothesized that a monoclonal antibody against a cell surface protein preferentially expressed on all NK cells, but only a minor subset of T cells, would efficiently deplete NK cells in the mouse lung and human blood cells and would blunt injury in mouse experimental and human *in vitro* models of IRI.

RESULTS

Human RNA sequencing screen of PGD BAL cells identifies KLRD1 as rational NK cell target.

Bronchoalveolar lavage (BAL) was collected on the 1st postoperative day after lung transplantation and cells from participants with severe PGD (n = 20) and those without PGD (n= 18) underwent RNA sequencing, as reported previously [12]. To identify a plausible marker for NK cell targeting, we performed a genomic screen of 18 NK cell-associated transcripts using a random forest model to predict severe PGD with leave one out validation. The model had high sensitivity and specificity (AUC ROC, 0.76, 95% Confidence Interval [CI], 0.61-0.91) with accuracy displayed in a receiver operator curve plot (**Figure 1A**). We found that *KLRD1*, encoding the CD94 surface protein, had the highest feature importance across the 18 NK cell genes (**Figure 1B**). We investigated *KLRD1* gene transcript counts and found that *KLRD1* was increased in BAL from recipients with severe PGD compared to recipients without PGD (**Figure 1C**, p = 0.02). We stratified this cohort by PGD status and median of *KLRD1* gene counts from the group without PGD. We found *KLRD1*^{hi}PGD participants had an 8.5-fold increased risk (95% CI 3.2-22.2, p< 0.0001) for ICU care after transplantation as compared to the other participants (**Figure 1D**). These data identify CD94 as a rational target against NK cells that may be exploited to modulate PGD risk.

Mouse pulmonary CD94+ NK cells co-express NKG2A and are activated.

CD94 is covalently bonded to the NKG2A or NKG2C proteins forming a heterodimeric receptor that recognizes non-classical MHC I (HLA-E in humans and Qa-1 in mice)[24]. Because CD94/NKG2A+ NK cells in the mouse lung have not been fully characterized, we measured CD94 and NKG2A on cells in the blood, spleen, and lung from C57BL/6 mice (n = 6, **Supplemental Figure 1**). We found that CD94+ NK cells had high expression of NKG2A (**Figure 2A**). NKG2A+ NK cells comprised nearly 100% of the CD94+ population and median fluorescence intensity of CD94 was similar on NK cells in the blood, spleens, and lungs of mice (**Figures 2B & 2C).**

To understand the potential impact of anti-CD94 monoclonal antibody treatment, we examined immunophenotypes of NKG2A+ and NKG2A- NK cells from C57BL/6 mice (n = 10) in blood, spleen, thoracic lymph nodes, and lungs (**Figure 2D).** Across all tissues, NKG2A+ NK cells comprised a median 44.8%(interquartile range [IQR] 42.3 – 47.8%) of the total NK cell population (**Figure 2E**). CD11b and CD27 are acquired NK cell markers of maturation progressing to CD11b+CD27- NK cells (**Figure 2F**). We found that NKG2A+ NK cells were immature and had higher expression of CD27 than NKG2A- NK cells (**Figures 2G-2J**). We also measured 15 additional markers on lung NK cells **(Figure 2K).** We found no differences in Ly6c, CXCR4, CXCR6, CCR2, Ly49CI, or CD69. Notably, in tissues, NKG2A+ NK cells had increased CD49a, a marker of tissue residency. DNAM1 and KLRG1, markers of activation,

were also increased in the NKG2A+ population relative to NKG2A- NK cells. NKG2A+ NK cells had increased chemokine receptors (CCR5, CXCR2, CXCR3) and CD62L, suggesting a circulating source for some of this population. Together, these data suggest that anti-CD94 monoclonal antibody treatment would target an immature or activated subset of NK cells that comprise roughly half of the pulmonary NK cell niche.

Mouse NKG2A+ NK cells are increased, activated and tissue-resident during IRI.

To understand the pulmonary NKG2A+ NK cell profile during warm IRI (**Figure 3A**), where lungs are not exposed to static cold storage, we investigated differences in the most prevalent markers following hilar clamp (HC, n = 7) and sham procedures (S, n = 7). Overall, the frequency of NKG2A+ NK cells was increased in the lung following HC as compared to sham thoracotomy (**Figure 3B,** p = 0.04). Notably, tissue-resident NKG2A+ NK cells were increased in HC lungs (**Figures 3C & 3D**) compared to sham lungs (p = 0.002). DNAM1, a marker of NK cell activation, was also increased during lung IRI (**Figures 3E & 3F,** p=0.05), but no differences were observed in KLRG1 expression (Figures 3G & 3F). These data suggest that IRI leads to a skewed NKG2A+ NK cell population described by increased frequencies of tissue-resident and activated cells.

Anti-mouse Anti-CD94 treatment reduces lung NK cells

We hypothesized that CD94-based depletion would reduce lung NK cells following warm IRI (**Figure 4A**). To test this hypothesis, we generated an anti-mouse anti-CD94 monoclonal antibody (**Supplemental Figures 2A-2D**). This antibody demonstrated high affinity for CD94 antigen (**Supplemental Figure 2E)** and high staining of CD94-transuced mouse Ba/F3 cells (**Supplemental Figure 2F**).

As expected, anti-mouse anti-CD94 monoclonal antibody-treated mice had reduced frequencies of lung NK cells compared to isotype-matched control IgG-treated mice (p = 0.004) and sham mice (p = 0.03, **Figures 4B and 4C**). As the airways and alveoli are primary sites of injury within this model, we examined BAL separately from lung tissue. Absolute BAL NK cells were reduced in the anti-mouse anti-CD94 monoclonal antibody group when compared to isotype-matched IgG-treated mice (p = 0.04, **Figure 4D**). We found no significant differences in the minority of NK cells in the BAL that express CD49a (**Figure 4E**). However, anti-CD94 treatment markedly reduced the overall CD49a+ NK cells in the lung (**Supplemental Figure 3A**, p = 0.001) during IRI. In addition, anti-CD94 treatment reduced the CD49a+NKG2A+ subsets in the lung (**Supplemental Figure 3B**) and BAL (**Supplemental Figure 3C & 3D**). Altogether, these data indicate that anti-CD94 antibodies can effectively penetrate the airway, alveolar, and lung tissue compartments.

Other lymphocytes, specifically minor subsets of T cells, can express NK receptors, including NKG2A [25]. Therefore, we measured the depletion efficiency of CD8 and γδ T cells within the lung. We found no differences in depletion in CD8+ T cell (**Figure 4F,** p = 0.3) or γδ T cells (**Figure 4G,** p = 0.8) across the 3 conditions. We examined NKG2A+ populations across all NK cells within the lung (**Figure 4H**). As expected, the frequency of NKG2A+ NK cells were significantly reduced in the anti-mouse anti-CD94 monoclonal antibody group (3.5 IQR 2.9 – 7.7%) compared to both the isotype-matched IgG-treated (38.2 IQR 34.7 – 44.2%, p = 0.004) and sham groups (45.8 IQR 28.8 – 47.1%, p = 0.004, **Figure 4I**). We also found that anti-mouse anti-CD94 monoclonal antibody resulted in reduced NKG2A+ lymphocytes compared to the other mice (**Figure 4J**). In summary, these data suggest that anti-mouse anti-CD94 monoclonal antibody treatment targets most lung NK cells but also the broad population of NKG2A-bearing lymphocytes.

Anti-mouse Anti-CD94 treatment blunts lung IRI damage

We previously reported that NK cells mediate pulmonary IRI in mice [13]. Here, we hypothesized that anti-mouse anti-CD94 NK cell depletion would reduce lung damage from warm IRI (**Figure 5A**). Representative H&E histopathology (n = 5 for each condition) from sham, isotype-matched IgG-treated HC, and anti-mouse anti-CD94 monoclonal antibody-treated HC lungs are shown in **Figure 5B**. We performed qualitative assessments of the histopathology[26]. Relative to sham mice, the lungs from isotype-matched IgG-treated HC mice had diffuse alveolar damage that was abrogated in the anti-mouse anti-CD94-treated HC lungs. Diffuse alveolar damage is characterized by neutrophilic infiltration, alveolar interstitial thickening, and pulmonary edema.

We quantified lung injury by measuring arterial oxygen (PaO2) and with radiolabeled albumin I^{125} to derive lung extravascular lung water, extravascular plasma equivalents and endothelial permeability. The anti-mouse anti-CD94-treated HC mice had significantly higher PaO2 (462 IQR 439 – 515 mmHg) relative to isotype-matched IgG-treated HC mice (323 IQR 256 – 377 mmHg, **Figure 5C**, p = 0.009) and similar PaO2 to sham-treated mice (622 IQR 592 – 647 mmHg, p = 0.34). We found comparable volumes of extravascular lung water (**Figure 5D**) between sham (16.7 IQR 10.8 – 20.5 uL) and anti-CD94-treated HC mice (24.8 IQR 18.6 – 28 uL, p = 0.34) with increased volumes within the isotype-matched IgG-treated HC mice (33.9 IQR 27.9 – 44, p = 0.004 and p = 0.02 respectively). There was a similar pattern of findings between the 3 groups for extravascular plasma equivalents (**Figure 5E**). Extravasation of albumin was reduced in anti-CD94 HC lungs compared to isotype-matched control Ig-treated HC lungs (**Figure 5F**, p = 0.01) but was increased relative to sham lungs (p = 0.05). Finally, we observed similar findings in endothelial permeability across the 3 groups (**Figure 5G**). Separately, we found no differences in PaO2 or histology between sham mice

treated with anti-CD94 antibody compared to those without antibody (**Supplemental Figure 4).**

Unlike the mouse model of hilar clamping-induced lung IRI, human lung transplantation is almost always allogeneic. To investigate the effect of anti-CD94 treatment on IRI in allogeneic conditions, we assessed the effect of anti-CD94 versus isotype treatment in C57BL/6 (B6, MHC type: H-2^b) recipients given orthotopic lung allografts from H-2^d C57BL/6 (B6.*H2^d*, MHC type: H-2^d) mice following 4 hours of cold ischemic time (n = 5, **Figure 5H**). Anti-mouse anti-CD94 treatment resulted in effective NK cell depletion relative to isotype-control (**Figure 5I**, p = 0.02). NKG2A+ NK cells (**Figure 5J,** p = 0.008) and NKG2A+ lymphocytes in general (**Figure 5K,** p = 0.008) were efficiently depleted in anti-mouse anti-CD94-treated group. Injury to the allografts was quantified by assessing quantitative pathology scores, BAL protein content, and arterial PaO_2. The anti-mouse anti-CD94-treated transplants had a trend toward lower pathology score (**Figures 5L & 5M,** p = 0.08), lower BAL protein content (**Figure 5N,** p = 0.03), and higher PaO_2 (**Figure 5O,** p = 0.03). Together, data from two mouse models of IRI suggest that CD94-based depletion reduces quantitative and qualitative measures of lung damage after IRI.

Anti-human anti-CD94 therapy reduces human airway cytotoxicity via NK cell depletion

To evaluate the effects of CD94-targeted depletion in humans, we characterized CD94 expression on T cells and NK cells from lung transplant recipient PBMCs. NK cells and T cells were enumerated (**Figure 6A**). We observed higher frequency of CD94 expression on NK cells as compared to CD45+CD3+ T cells **(Figure 6B**). Specifically, only median 16.3% (IQR 16 - 29.8%) of the CD8 T cells were $CD94^+$ (p = 0.004, **Figure 6C**), whereas 79% (IQR 77 - 85.7%) of the NK cells were $CD94^+$ (p = 0.0005, **Figure 6D**). We surmised that anti-human anti-CD94 treatment of human PBMCs could deplete up to 80% of the human NK cell population.

To understand the specific phenotypes of lung lymphocytes in patients with PGD, we characterized NK cell markers on BAL cells from human lung transplant recipients in the first 2 weeks after transplantation. Baseline characteristics for this cohort are shown in **Supplemental Table 1**. BAL NK cells had high frequencies of CD94 expression (86.7% IQR 77.8 - 90.5%**, Figure 6E,** p = 0.0005). We stratified NK cells by CD94 and PGD status (**Figure 6F**) and found that BAL $CD94^{hi}$ NK cells from recipients with PGD had increased NKG2D as compared to no PGD $CD94^{hi}$ populations (**Figures 6F and 6G**). We concluded that by using an anti-CD94-targeted depletion strategy, we would also be depleting a majority of the NKG2D+ NK cells.

We also investigated CD94 expression on BAL T cells. Nearly all CD4 T cells in the BAL lacked CD94 (**Supplemental Figure 5A,** p < 0.0001). CD8 T cells in the BAL had

heterogeneous CD94 expression, with nearly equal $CD94^{low\ (or\ negative)}$ and $CD94^{hi}$ expression (**Supplemental Figure 5B**, p = 0.3). We observed increased NKG2D on $CD94^{hi}$ CD8 T cells (p = 0.8), but little NKG2D expression on CD4 T cells (**Supplemental Figure 5C**). Thus, a CD94-targeted depletion strategy would be expected to deplete CD8 BAL T cells but largely spare the CD4 T cell compartment.

We assessed the *in vitro* depletion efficacy of anti-human anti-CD94 monoclonal antibody in recipient PBMCs relative to isotype-matched control antibody (**Figure 6H**)[27]. Compared to isotype-matched control IgG, PBMCs treated with $>1x10^{-5}$ ug/uL of anti-CD94 had reduced frequencies of NK cells (**Figures 6I & 6J**). Based on the EC_{50} of $1.3x10^{-4}$ ug/uL, a concentration of 0.1 ug/ul anti-CD94 monoclonal antibody was set as the effective NK cell depletion dose.

We further hypothesized that anti-human anti-CD94 antibody would reduce killing in our *in vitro* cultures employing hypoxic airway epithelial cells to model IRI. Following 24 hours of hypoxia (1% O_2) epithelial cells were co-cultured with lung transplant recipient PBMCs pre-treated with anti-CD94 monoclonal antibody or isotype-matched IgG control (**Figure 6K**). Airway epithelial cells were identified via cell tracer and cytotoxicity was determined by viability (**Supplemental Figure 6**). There was reduced killing of hypoxic epithelial cells with anti-human anti-CD94 monoclonal antibody treatment compared to isotype-matched control IgG treatment (p = 0.04, **Figure 6L & 6M**). These data suggest that anti-human anti-CD94-targeted therapy is effective at reducing airway epithelial killing, a key surrogate of human PGD.

Anti-mouse CD94-targeted depletion did not affect donor antigen-presenting cells in the allogeneic orthotopic lung transplant model

NK cells have been shown to enhance lung allograft tolerance in an orthotopic lung transplant (OLT) model of acute and chronic T cell-mediated rejection via selective depletion of donor antigen presenting cells (APCs) [28]. It is unknown how NK cell depletion may modulate long-term allogeneic lung allograft outcomes, independently from IRI. We hypothesized that anti-CD94 NK cell depletion would not alter long-term tolerance in an allogeneic OLT model. Therefore, we treated recipient mice with intraperitoneal isotype-matched IgG control antibody (n = 5), anti-mouse anti-CD94 antibody (αCD94, n = 4)**,** or IL-15 receptor complex (IL15RC, n = 4) 1-hour preceding BALB/c allogeneic donor OLT with minimal warm ischemia (MWI, no IRI) and measured outcomes at 3 days (**Figure 7A**). IL-15RC was used to stimulate NK cells as a positive control. We found that anti-mouse anti-CD94 antibody reduced lung NK cells (**Figure 7B**, p = 0.02), most profoundly in the NKG2A+ population (**Figure 7C**, p = 0.0001) relative to isotype-matched IgG treatment. As expected, we found reduced donor APCs in IL15RC mice compared to isotype-matched IgG-treated mice (**Figure 7D,** p = 0.02). Anti-mouse anti-CD94 antibody had no impact on donor APCs

relative to control ($p = 0.83$). We observed no differences in PaO2 (**Figure 7E**), BAL protein (**Figure 7F**), or cell-free DNA (**Figure 7G**) across the 3 groups.

NK cell depletion in a mouse allogeneic orthotopic lung transplant model does not alter graft acceptance

In addition to a role in allograft tolerance, NK cells have also been shown to mediate obliterative airway disease in an allogeneic heterotopic tracheal transplant model in an NKG2D-dependent fashion [29]. It is unknown how NK cell depletion would alter lung pathology in the allogeneic OLT model as tracheas lack the complexity of the lung. Therefore, we assessed 4 different histopathology measures 14 days following transplantation of an untreated isograft or allografts treated with isotype-matched IgG-control antibody, anti-mouse anti-CD94-based depletion, or IL-15 receptor complex (**Figure 7H**). Representative H&E images are shown **in Figure 7I** and **Supplemental Figure 7.** We found that IgG-treated lungs had increased inflammation by nuclei counted per high-powered field (**Figure 7J,** $p = 0.01$) and surrounding airways (**Figure 7K,** $p = 0.03$) relative to isografts. There was also reduced airway patency (**Figure 7L,** $p = 0.01$) and increased pleural thickness in the control IgG-treated lungs (**Figure 7M,** $p = 0.03$) relative to isografts. Notably, anti-mouse anti-CD94 monoclonal antibody treatment blunted inflammation around airways relative to IgG-treated mice ($p = 0.03$) and IL15RC had no impact on any of these measures. Together, these suggest a trend to reduced chronic inflammation with NK cell depletion.

DISCUSSION

Here, we describe a novel approach to target an important innate immune cell implicated in the pathogenesis of pulmonary ischemia reperfusion injury (IRI). We show that CD94 is abundant on mouse and human NK cells and that a monoclonal antibody efficiently depletes >50% of lung NK cells in the mouse. In mouse and human experimental models, we find that CD94 depletion is effective at reducing lung injury and airway epithelial cell killing, respectively. These findings represent a critical step towards clinical NK cell depletion.

There are key differences in NK cell receptor repertoires between mice and humans. While both species express CD94, it is expressed on ~50% of mouse NK cells, while it is found on most human NK cells as a bimodal population of $CD94^{dim}$ and $CD94^{bright}$ [30-32]. This explains the roughly 50% depletion efficiency we observed in the mouse. Compared to historic published data, anti-NK1.1-based treatment resulted in almost complete NK cell depletion due to expression of NK1.1 on all mouse NK cells and, concordantly, achieved nearly twice the reduction in injury relative to our observations here [13]. Nonetheless, we observed clinically significant reductions in mouse lung injury with CD94 depletion. In humans, we found nearly 80% of lung transplant recipient circulating and BAL NK cells expressed CD94 and would expect a greater reduction in NK cells with *in vivo* depletions compared to the mouse. NK cell *in vitro* depletions could potentially be limited by reduced sources of cytokines and viability of cells due to cryopreservation, resulting in diminished antibody-dependent cell-mediated cytotoxicity.

NK cell depletion, rather than receptor blockade, may carry broader repercussions as NK cells participate in a variety of other mechanisms that may impact lung transplant outcomes. Our observations that CD94+ NK cells in the BAL of recipients with PGD have increased NKG2D receptor expression suggest that CD94-based depletion may preferentially target this critical sub-population of NK cells. Consequently, in skin and lung, NK cells have been shown to support early allograft acceptance via selective depletion of donor APC [28, 33]. It was unknown if one-time NK cell depletion at induction would alter this effect. Here, we find that while NK cell stimulation via IL-15-IL-15 receptor complexes augments donor APC killing, CD94-based depletion had no impact on donor APCs relative to control animals, likely because half of the NK cells were depleted. We also found no detrimental effect of NK cell depletion on chronic graft injury, suggesting that selective depletion of CD94 subsets does not impact this APC-dependent tolerance mechanism. Notably, NK cells play a central role in mitigating human and mouse cytomegalovirus infection [34-37]. However, we previously reported that the CMV-specific NK cell populations bearing NKG2C receptors may be deleterious following lung transplantation [38]. NK cells may also mediate chronic lung allograft dysfunction through NKG2D-mediated recognition of stress molecules on small airway cells [29]. Finally, NK cells are key mediators of antibody-mediated transplant rejection

via antibody dependent cell-mediated cytotoxicity [39-42]. While we have shown that selective CD94-based NK cell depletion blunts acute injury following ischemia-reperfusion with minimal impact on tolerance, further work is required to determine if depletion may impact these other important endpoints.

A particular strength of this study is the concordance of findings within two established mouse models of IRI and in an *in vitro* human model of airway cell killing. In addition, we modeled and replicated an important mechanism of NK cell tolerance and demonstrated no large differences in long-term outcomes with CD94-based NK cell depletion versus positive and negative control conditions. Another important limitation is that the *in vitro* human model of airway cell killing used recipient cells from the circulation rather than bronchoalveolar lavage as there are too few lymphocytes in these samples for these experiments. While tissue-specific functional differences may be unaccounted for in this study, we previously reported that most NK cells responding to lung IRI are from the circulation [13]. This study focused on NK cells, but CD94 is expressed in lower frequencies on T cells [43]. As such, the results observed from CD94-based depletion may not be due to impacts on NK cell populations alone.

These findings have broad implications outside of lung transplantation. Notably, existing studies have identified NK cells and hypoxia signaling as important transcriptional pathways in acute respiratory distress syndrome (ARDS) patients with bacterial lower respiratory infections [44, 45]. In kidney IRI, NK cells have also been shown to mediate damage through NKG2D activation [46-48]. Together, these data suggest that CD94-based depletion strategies may be beneficial in other acute injury syndromes.

In conclusion, we describe a novel and efficacious approach to deplete NK cells prior to pulmonary IRI. These findings represent a critical intermediary step to a human trial of CD94-based NK cell depletion in lung transplantation to prevent PGD. Such a strategy may rationally be included in induction therapy.

ACKNOWLEDGEMENTS

We thank Jeff Golden, Mary Ellen Kleinhenz, Lorianna Leard, Rupal Shah, Nicholas Kolaitis, Aida Venado and the other members of the clinical lung transplant team for their care of our patients and design of the clinical protocols. We thank Fengchun Liu for his work on the hilar clamp model system. We are thankful for the cooperation of Donor Network West, for all the organ and tissue donors, and their families for giving gifts of life and knowledge with their generous donation.

The authors report partial project funding with support from Dren Bio. DRC receives salary support from the CFF (CALABR19Q0) and VA ORD BLRD (1IK2BX005301). JRG receives salary support from CFF, VA ORD(CX002011), and NIH (HL151552). L.L.L. is supported by the Parker Institute for Cancer Immunotherapy (PICI) and NIH (AI068129). MRL and JPS were supported by the NIH (R01HL130324) and MRL was supported by the NIH (R35HL161241). We acknowledge the Parnassus Flow Cytometry Core (RRID:*SCR 018206*) supported in part by Grant NIH P30 DK063720 and by the NIH S10 Instrumentation Grant S10 1S10OD026940-01. The animal microsurgery core was also supported by the Nina Ireland Program for Lung Health.

AUTHOR CONTRIBUTIONS

Conceptualization: DRC, LLL, JRG, RS, JR
Methodology: DRC, TT, LB, SC
Investigation: DRC, TT, LQ, AS, AMH, LB, RB, JPS, JasleenK, JeffreyK, AS, TS, SC, NG, DZ
Data Analysis: DRC, TT, KB, RS, RB, NG
Visualization: DRC
Funding acquisition: DRC, MRL, JPS
Writing – original draft: DRC
Writing – review & editing: DRC, LLL, JRG, MRL, JPS, RS, JS, KD, MW, NT, TT

DECLARATION OF INTERESTS

We the authors declare that Ruoshi Shi, Lu Bai, Kimberly Dilley, Mattias Will, Nenad Tomasevic, Tereza Sputova, Adam Salles, and Jeffrey Kang are employees and shareholders of Dren Bio, Inc. Nenad Tomasevic is a founder and holds a management position at Dren Bio, Inc. Matthias Will holds a management position at Dren Bio, Inc. Lewis L. Lanier is a consultant for Dren Bio, Inc. The authors have no additional conflicts to disclose.

METHODS

Mice

Male C57BL/6J (#000664), BALB/cJ (#000651), and C57BL/6J CD45.1 (B6.SJL-*Ptprc*^{a} *Pepc*^{b}/BoyJ, #002014) mice weighing 25–30 grams were purchased from Jackson Laboratories (Bar Harbor, ME). B6.C-*H2*^{d}/bByJ (B6.*H2*^{d}, #000359) mice originated from Jackson Laboratories and were bred and maintained at UCSF[49]. Mice were housed in a pathogen-free barrier facility and experiments were conducted according to protocols approved by the UCSF Institutional Animal Care Use Committee.

Experimental models of lung IRI and lung transplantation

Warm IRI was performed by an experienced microvascular surgeon, as previously described [13, 25, 50]. After anesthetization, mice underwent a left thoracotomy, then a slipknot suture was tied around the left hilum (hilar clamp, HC) or left untied as a sham surgery (S). The suture was removed after 2 hours of ischemia, and animals were euthanized after 4 hours of reperfusion. Mice were treated 24 hours preceding IRI surgery with 10 mg/kg of anti-mouse anti-CD94 antibody (Dren Bio, CA) or 10 mg/kg of anti-mouse IgG2a isotype-matched control (Clone C1.18.4, BioXCell, BP0085). Single left lung bronchoalveolar lavage was performed by gently lavaging 300 uL of PBS. BAL, bilateral lungs, and blood were collected for analysis.

We also performed allogeneic orthotopic lung transplantation with minimal warm ischemia (OLT-MWI) without immunosuppression to assess the chronic rejection of obliterative airway disease [51]. Left BALB/c donor lungs were procured and transplanted into C57BL/6 or C57BL/6 CD45.1 recipient mice using interrupted sutures for the anastomoses. Recipient mice received 10 mg/kg of anti-mouse anti-CD94 antibody (Dren Bio, CA), 10 mg/kg of anti-mouse IgG2a isotype-matched control (Clone C1.18.4, BioXCell, BP0085), or 0.4 mg/kg of IL-15-IL-15 receptor complex 1 hour before OLT-MWI. IL15 was complexed prior to injection by mixing 1.5ug of mouse recombinant IL-15 (R&D Systems, 447ML010CF) with 10.05 ug of mouse recombinant IL-15Rα-Fc (R&D Systems, 551MR100) and incubated at 37°C for 20 minutes. As a negative control, we also performed syngeneic orthotopic left lung transplantation from a C57BL/6 donor to a C57BL/6 recipient with minimal warm ischemia (isograft). The recipient animals were euthanized 3 days or 14 days after transplantation. The left and right lungs and blood were collected for analysis.

We also performed allogeneic orthotopic lung transplantation with cold ischemia (OLT-CI) without immunosuppression to assess IRI in a setting more closely approximating human lung transplantation. Left lungs from B6.H2^{d} mice, congenic except at the MHC locus, were procured, perfused with 1ml of heparinized saline, covered with a saline-soaked gauze, and placed at 4°C for 4 hours of cold ischemia before being transplanted into C57BL/6 recipient

mice using the same surgical method detailed above for the allogeneic OLT-MWI. Donor and recipient mice received 10 mg/kg of anti-mouse anti-CD94 antibody (Dren Bio, CA) or 10 mg/kg of anti-mouse IgG2a isotype-matched control (Clone C1.18.4, BioXCell, BP0085) 24 hours before OLT-CI. The recipient animals were euthanized 20 hours after transplantation. The left lung was collected for analysis.

Acute lung injury measurements and lung digestion

We assessed lung vascular permeability to ^{125}I-labeled albumin (Jeanatope, Iso-Tex Diagnostics, Pearland, TX), gamma counts of ^{125}I-labeled albumin per gram of dried lung, and arterial PaO_2 as previously described [13, 50]. Endothelial permeability was calculated by quantifying the clearance of ^{125}I-labeled albumin across the endothelium and into extravascular space as previously described [52, 53]. Lung samples for histopathology were collected in 1% paraformaldehyde (#047392.9M, ThermoFisher), stored in 70% ethanol before paraffin embedding, sectioning, and hematoxylin and eosin (H&E) staining. Slides were scanned with a Zeiss Axio ScanZ.1 microscope and digitally assessed with ImageJ software [54]. Lungs were placed into 1 mL PBS with 10 µL of 10 µg/µL collagenase D (Sigma-Aldrich, # 11088858001) and 10 µL of 10 µg/µL DNAse I (#10104159001, Sigma-Aldrich), dissociated, and processed as previously described [13].

Anti-mouse anti-CD94 monoclonal antibody production and purification

The antibody sequence vector and plasmid DNA were constructed using the pCDNA3.4 kit (ThermoFisher, #A14697). Antibody variable light gene and variable heavy gene were cloned into pFUSE2-CLIg-hK (Invivogen, #pfuse2-hclk) and pFUSE-CHIg-hG1 (Invivogen, #pfusehchg1), respectively (**Supplemental Figures 2A and 2B**). Cloning was done by Genscript (Piscataway, NJ). A HEK-293 (Invitrogen, Carlsbad, CA) cell line lacking fucosyl transferase (293-NF) was used to produce non-fucosylated antibody. 293-NF and suspension HEK-293 cells were co-transfected with expression plasmid containing genes encoding the heavy chain and the light chain in a 1:1 ratio using an ExpiFectamine 293 Transfection Kit (ThermoFisher, #A14524) according to the manufacturer's recommendations. Cells were collected 5 days after transfection and cell culture fluid was obtained through centrifugation and sterile filtration. Cell culture fluid was purified using a Protein A affinity chromatography column on an AKTA Pure 150 (Cytiva, Marlborough, MA). Protein concentration was determined by UV-absorbance at 280 nm. Monomer content was determined by high performance liquid chromatography size exclusion using a HiLoad Superdex 200 column (Cytiva, **Supplemental Figure 2C**). Glycan distribution across fucosylated and non-fucosylated antibodies was determined with the Glycan Profiling Assay Release Kit (PerkinElmer, #CLS155434, **Supplemental Figure 2D**). Binding of the antibody to mouse

CD16a and mouse CD94 were measured by Biolayer Interferometry (BLI) on an Octet (Sartorius, Ann Arbor, Michigan, **Supplemental Figure 2E**). To assess antibody affinity for antigen bound to the cell surface, mouse CD94-transduced Ba/F3 cells were generated (Lewis L. Lanier)[14]. Anti-mouse CD94 antibody was titrated with 3-fold dilutions and incubated with CD94+ Ba/F3 cells for 30 minutes followed by staining with 1:300 dilution of AffiniPure Goat Anti-Mouse IgG, Fcγ fragment specific Alexa fluor 647 secondary antibody (Jackson Immunoresearch, # 115-605-071). Data were acquired on a CytoFlex LX flow cytometer (Beckman Coulter, Brea, CA) and MFI values were obtained with FlowJo (Ashland, Oregon, **Supplemental Figure 2F**).

BAL protein quantification

BAL fluid was centrifuged at 300 x g for 10 minutes at 4°C to pellet cells. Isolated BAL supernatant was stored at -80°C as recommended by the assay kit manufacturer. Protein quantification was done using the BCA assay kit (Pierce BCA Protein Assay Kit, #23225, ThermoFisher) according to the manufacturer's instructions.

Cell-free DNA quantification

Blood was collected from mice using EDTA-coated tubes to prevent coagulation. Blood was mixed gently by inverting the tube a few times to ensure thorough mixing with the anticoagulant. Blood collecting tubes were centrifuged at 1,600 x g for 10 minutes at 4°C to separate the plasma from cellular components. Plasma was collected (top layer) into a 2 mL microcentrifuge tube without disturbing the buffy coat or red blood cell layer and cfDNA isolation from blood plasma were done according to MagMAX Cell free DNA isolation kit (ThermoFisher, # A29319). Isolated cfDNA was quantified using Qubit HSDNA Assay Kit.

Mouse lung immunophenotyping

Lung cell suspensions were washed and incubated at 37°C with anti-mouse anti-CD16+CD32 (BioLegend, # 101320) to block non-specific binding and stained with viability exclusion dye. Cells were further stained with the remaining fluorophore-conjugated antibodies at 4°C and washed. Antibody panels and gating strategies are detailed for 4 different flow cytometry panels used to: 1) immunophenotype CD94+ NK cells at rest (**Supplemental Table 2, Supplemental Figure 1),** 2) assess NKG2A+ NK cells during IRI **(Supplemental Table 3, Supplemental Figure 1),** 3) quantify NK cells during IRI depletion experiments **(Supplemental Table 4, Supplemental Figure 1),** and 4) measure donor antigen presenting cells following allogeneic OLT-MWI **(Supplemental Table 5, Supplemental Figure 8).** Data were acquired on BD Biosciences LSR II and LSR Fortessa

flow cytometers, respectively. Flow cytometry data were visualized and analyzed with FCS express (De Novo Software, Pasadena, CA).

Human in vitro NK cell depletion and airway epithelial cell co-culture experiments

Human samples were collected from consenting adults. Peripheral blood mononuclear cells (PBMCs) from 5 lung transplant recipients who underwent lung transplantation at the University of California, San Francisco (UCSF) were obtained within the first year after transplantation. **Supplemental Table 6** shows baseline characteristics for this cohort. NK cells, CD4 T cells, and CD8 T cells were quantified with flow cytometry (**Supplemental Table 7**) before and after treatment with anti-βgal human IgG1 isotype-matched control antibody (InvivoGen, #bgal-mab13) and anti-human anti-CD94 monoclonal antibody (Dren Bio) across a range of concentrations from $1x10^{-6}$ ug/mL to 10 ug/mL.

To assess airway epithelial cell cytotoxicity, human bronchial epithelial cells (16HBE14o-, Sigma Aldrich, SCC150) were plated and allowed to adhere overnight. They were then exposed to hypoxia (1% O_2) for 24 hours and then co-cultured in a 2:1 effector-to-target ratio with PBMCs treated with IgG isotype-matched control antibody or anti-CD94 antibody for an additional 24 hours. Airway epithelial cells were stained with CellTrace Violet (Invitrogen, C34557) prior to plating to distinguish PBMCs from epithelial cells. Upon collection, cells were stained with Fixable Viability Dye eFluor 660 (Invitrogen, 65-0864-14) and data were collected on a BD FACSAria Fusion flow cytometer.

Human lung transplant BAL RNA sequencing and immunophenotyping

Bronchoalveolar lavage was collected on the first post-transplant day from consenting lung allograft recipients at 2 centers through a previous study [12]. RNA sequencing was performed on the BAL cell pellet as previously described [12]. **Supplemental Table 8** shows the baseline characteristics for this cohort, which contains 2 additional samples from the previously published cohort. All studies of human samples were conducted according to approved institutional review board protocols.

As previously reported, we also collected bronchoalveolar lavage from lung transplant recipients with severe PGD (n = 5) and those without PGD (n = 7) within 2 weeks of lung transplantation (**25**). Samples from recipients with PGD were matched based on age, sex, transplant indication, and ethnicity to no-PGD recipient samples. **Supplemental Table 1** shows the baseline characteristics for the recipients included in these analyses.

Statistical analyses

Experimental data were tested for normality with Shapiro-Wilk tests. Comparisons of means in experiments with multiple groups were made with Kruskal-Wallis test or ANOVA, and *post-*

hoc differences were assessed with 2-tailed Mann-Whitney U tests or Student's t-tests, as appropriate. All tests were adjusted for multiple comparisons with the Benjamini-Hochberg approach. Differences between NK cell surface markers were determined with paired testing. Results were visualized using box and whisker plots showing individual data points bound by boxes at 25^{th} and 75^{th} percentiles and medians depicted with bisecting lines. RNA sequencing NK cell genetic screen was performed with a random forest model using 18 NK cell genes as predictors of severe PGD with leave one out validation. The model results were visualized via feature plot relative importance and the model's fit was tested with area under the curve of the receiver operator curve (AUC ROC). A p-value <0.05 was considered significant. Analyses and plotting were performed in R (R Foundation for Statistical Computing, Vienna, Austria).

Study approval

The UCSF institutional review board approved the human subject components of this study under protocol 13–10738. Written informed consent was obtained from all participants prior to inclusion in the study. All animal procedures and experiments were conducted according to protocols approved by the UCSF Institutional Animal Care Use Committee.

REFERENCES

1. Valapour M, Lehr CJ, Schladt DP et al. OPTN/SRTR 2021 Annual Data Report: Lung. Am J Transplant 2023;23(2 Suppl 1):S379-s442.
2. Diamond JM, Lee JC, Kawut SM et al. Clinical risk factors for primary graft dysfunction after lung transplantation. Am J Respir Crit Care Med 2013;187(5):527-534.
3. Snell GI, Yusen RD, Weill D et al. Report of the ISHLT Working Group on Primary Lung Graft Dysfunction, part I: Definition and grading; A 2016 Consensus Group statement of the International Society for Heart and Lung Transplantation. J Heart Lung Transplant 2017;36(10):1097-1103.
4. Kolaitis NA, Gao Y, Soong A et al. Primary graft dysfunction attenuates improvements in health-related quality of life after lung transplantation, but not disability or depression. Am J Transplant 2021;21(2):815-824.
5. Paraskeva MA, Borg BM, Paul E et al. Abnormal one-year post-lung transplant spirometry is a significant predictor of increased mortality and chronic lung allograft dysfunction. J Heart Lung Transplant 2021;40(12):1649-1657.
6. Li D, Weinkauf J, Kapasi A et al. Baseline lung allograft dysfunction in primary graft dysfunction survivors after lung transplantation. Respir Med 2021;188:106617.
7. Morrison MI, Pither TL, Fisher AJ. Pathophysiology and classification of primary graft dysfunction after lung transplantation. J Thorac Dis 2017;9(10):4084-4097.
8. Cantu E, Diamond JM, Cevasco M et al. Contemporary trends in PGD incidence, outcomes, and therapies. The Journal of Heart and Lung Transplantation 2022;41(12):1839-1849.
9. Bharat A, Kreisel D. Immunopathogenesis of Primary Graft Dysfunction After Lung Transplantation. Ann Thorac Surg 2018;105(3):671-674.
10. Calabrese DR, Lanier LL, Greenland JR. Natural killer cells in lung transplantation. Thorax 2019;74(4):397-404.
11. Kumar S. Natural killer cell cytotoxicity and its regulation by inhibitory receptors. Immunology 2018.
12. Calabrese DR, Tsao T, Magnen M et al. NKG2D receptor activation drives primary graft dysfunction severity and poor lung transplantation outcomes. JCI Insight 2022;7(24):e164603.
13. Calabrese DR, Aminian E, Mallavia B et al. Natural killer cells activated through NKG2D mediate lung ischemia-reperfusion injury. J Clin Invest 2021;131(3):e137047.
14. Aguilar OA, Qualls AE, Gonzalez-Hinojosa MDR et al. MICB Genomic Variant is Associated with NKG2D-mediated Acute Lung Injury and Death. Am J Respir Crit Care Med 2023.
15. Chandrashekaran S, Crow Pharm SA, Shah SZ et al. Immunosuppression for Lung Transplantation: Current and Future. Curr Transplant Rep 2018;5(3):212-219.
16. Shagabayeva L, Osho AA, Moonsamy P et al. Induction therapy in lung transplantation: A contemporary analysis of trends and outcomes. Clin Transplant 2022;36(11):e14782.
17. Meehan AC, Mifsud NA, Nguyen TH et al. Impact of commonly used transplant immunosuppressive drugs on human NK cell function is dependent upon stimulation condition. PLoS One 2013;8(3):e60144.
18. Martin JF, Perry JS, Jakhete NR et al. An IL-2 paradox: blocking CD25 on T cells induces IL-2-driven activation of CD56(bright) NK cells. J Immunol 2010;185(2):1311-1320.
19. Groetzner J, Kur F, Spelsberg F et al. Airway anastomosis complications in de novo lung transplantation with sirolimus-based immunosuppression. J Heart Lung Transplant 2004;23(5):632-638.
20. Shemesh A, Su Y, Calabrese DR et al. Diminished cell proliferation promotes natural killer cell adaptive-like phenotype by limiting FcεRIγ expression. J Exp Med 2022;219(11).
21. Abel AM, Yang C, Thakar MS et al. Natural Killer Cells: Development, Maturation, and Clinical Utilization. Front Immunol 2018;9(1869).
22. Ryan JC, Turck J, Niemi EC et al. Molecular cloning of the NK1.1 antigen, a member of the NKR-P1 family of natural killer cell activation molecules. J Immunol 1992;149(5):1631-1635.

23. Vadstrup K, Bendtsen F. Anti-NKG2D mAb: A New Treatment for Crohn's Disease? Int J Mol Sci 2017;18(9):Available from doi: 10.3390/ijms18091997.
24. Iwaszko M, Bogunia-Kubik K. Clinical significance of the HLA-E and CD94/NKG2 interaction. Arch Immunol Ther Exp (Warsz) 2011;59(5):353-367.
25. Santos J, Wang P, Shemesh A et al. CCR5 drives NK cell-associated airway damage in pulmonary ischemia-reperfusion injury. JCI Insight 2023.
26. Matute-Bello G, Downey G, Moore BB et al. An official American Thoracic Society workshop report: features and measurements of experimental acute lung injury in animals. Am J Respir Cell Mol Biol 2011;44(5):725-738.
27. Shi K, Tan C, Bai L et al. DR-01, a Non-Fucosylated Anti-CD94 Antibody, Depletes Leukemic Cells in Ex Vivo and In Vivo Models of Large Granular Lymphocyte Leukemia. Blood 2022;140(Supplement 1):2259-2260.
28. Jungraithmayr W, Codarri L, Bouchaud G et al. Cytokine complex-expanded natural killer cells improve allogeneic lung transplant function via depletion of donor dendritic cells. Am J Respir Crit Care Med 2013;187(12):1349-1359.
29. Kawakami T, Ito K, Matsuda Y et al. Cytotoxicity of Natural Killer Cells Activated Through NKG2D Contributes to the Development of Bronchiolitis Obliterans in a Murine Heterotopic Tracheal Transplant Model. Am J Transplant 2017;17(9):2338-2349.
30. Borrego F, Masilamani M, Marusina AI et al. The CD94/NKG2 family of receptors. Immunol Res 2006;35(3):263-277.
31. Yu J, Mao HC, Wei M et al. CD94 surface density identifies a functional intermediary between the CD56bright and CD56dim human NK-cell subsets. Blood 2010;115(2):274-281.
32. Fang M, Orr MT, Spee P et al. CD94 is essential for NK cell-mediated resistance to a lethal viral disease. Immunity 2011;34(4):579-589.
33. Yu G, Xu X, Vu MD et al. NK cells promote transplant tolerance by killing donor antigen-presenting cells. J Exp Med 2006;203(8):1851-1858.
34. Adams NM, Geary CD, Santosa EK et al. Cytomegalovirus Infection Drives Avidity Selection of Natural Killer Cells. Immunity 2019;50(6):1381-1390.e1385.
35. Bayard C, Lepetitcorps H, Roux A et al. Coordinated expansion of both memory T cells and NK cells in response to CMV infection in humans. Eur J Immunol 2016;46(5):1168-1179.
36. Daniels KA, Devora G, Lai WC et al. Murine cytomegalovirus is regulated by a discrete subset of natural killer cells reactive with monoclonal antibody to Ly49H. J Exp Med 2001;194(1):29-44.
37. Lopez-Verges S, Milush JM, Schwartz BS et al. Expansion of a unique CD57(+)NKG2Chi natural killer cell subset during acute human cytomegalovirus infection. Proc Natl Acad Sci U S A 2011;108(36):14725-14732.
38. Calabrese DR, Chong T, Wang A et al. NKG2C Natural Killer Cells in Bronchoalveolar Lavage Are Associated With Cytomegalovirus Viremia and Poor Outcomes in Lung Allograft Recipients. Transplantation 2019;103(3):493-501.
39. Calabrese DR, Chong T, Singer JP et al. CD16+ natural killer cells in bronchoalveolar lavage are associated with antibody-mediated rejection and chronic lung allograft dysfunction. Am J Transplant 2023;23(1):37-44.
40. Loupy A, Duong Van Huyen JP, Hidalgo L et al. Gene Expression Profiling for the Identification and Classification of Antibody-Mediated Heart Rejection. Circulation 2017;135(10):917-935.
41. Parkes MD, Halloran PF, Hidalgo LG. Evidence for CD16a-Mediated NK Cell Stimulation in Antibody-Mediated Kidney Transplant Rejection. Transplantation 2017;101(4):e102-e111.
42. Toyoda M, Ge S, Suviolahti E et al. IFNgamma production by NK cells from HLA-sensitized patients after in vitro exposure to allo-antigens. Transpl Immunol 2012;26(2-3):107-112.
43. Arlettaz L, Villard J, de Rham C et al. Activating CD94:NKG2C and inhibitory CD94:NKG2A receptors are expressed by distinct subsets of committed CD8+ TCR alphabeta lymphocytes. Eur J Immunol 2004;34(12):3456-3464.
44. Sarma A, Christenson SA, Byrne A et al. Tracheal aspirate RNA sequencing identifies distinct immunological features of COVID-19 ARDS. Nat Commun 2021;12(1):5152.

45. Wesselkamper SC, Eppert BL, Motz GT et al. NKG2D Is Critical for NK Cell Activation in Host Defense Against Pseudomonas aeruginosa Respiratory Infection. J Immunol 2008;181(8):5481-5489.
46. Feng L, Cheng F, Ye Z et al. The effect of renal ischemia-reperfusion injury on expression of RAE-1 and H60 in mice kidney. Transplant Proc 2006;38(7):2195-2198.
47. Suarez-Alvarez B, Fernandez-Sanchez A, Lopez-Vazquez A et al. NKG2D and its ligands: active factors in the outcome of solid organ transplantation? Kidney Int Suppl (2011) 2011;1(2):52-57.
48. Victorino F, Sojka DK, Brodsky KS et al. Tissue-Resident NK Cells Mediate Ischemic Kidney Injury and Are Not Depleted by Anti-Asialo-GM1 Antibody. J Immunol 2015;195(10):4973-4985.
49. Cleary SJ, Kwaan N, Tian JJ et al. Complement activation on endothelium initiates antibody-mediated acute lung injury. J Clin Invest 2020.
50. Sayah DM, Mallavia B, Liu F et al. Neutrophil extracellular traps are pathogenic in primary graft dysfunction after lung transplantation. Am J Respir Crit Care Med 2015;191(4):455-463.
51. Krupnick AS, Lin X, Li W et al. Orthotopic mouse lung transplantation as experimental methodology to study transplant and tumor biology. Nat Protoc 2009;4(1):86-93.
52. Folkesson HG, Matthay MA, Hébert CA et al. Acid aspiration-induced lung injury in rabbits is mediated by interleukin-8-dependent mechanisms. J Clin Invest 1995;96(1):107-116.
53. Wiener-Kronish JP, Albertine KH, Matthay MA. Differential responses of the endothelial and epithelial barriers of the lung in sheep to Escherichia coli endotoxin. J Clin Invest 1991;88(3):864-875.
54. Schneider CA, Rasband WS, Eliceiri KW. NIH Image to ImageJ: 25 years of image analysis. Nature Methods 2012;9(7):671-675.
55. Chiossone L, Chaix J, Fuseri N et al. Maturation of mouse NK cells is a 4-stage developmental program. Blood 2009;113(22):5488-5496.

FIGURES

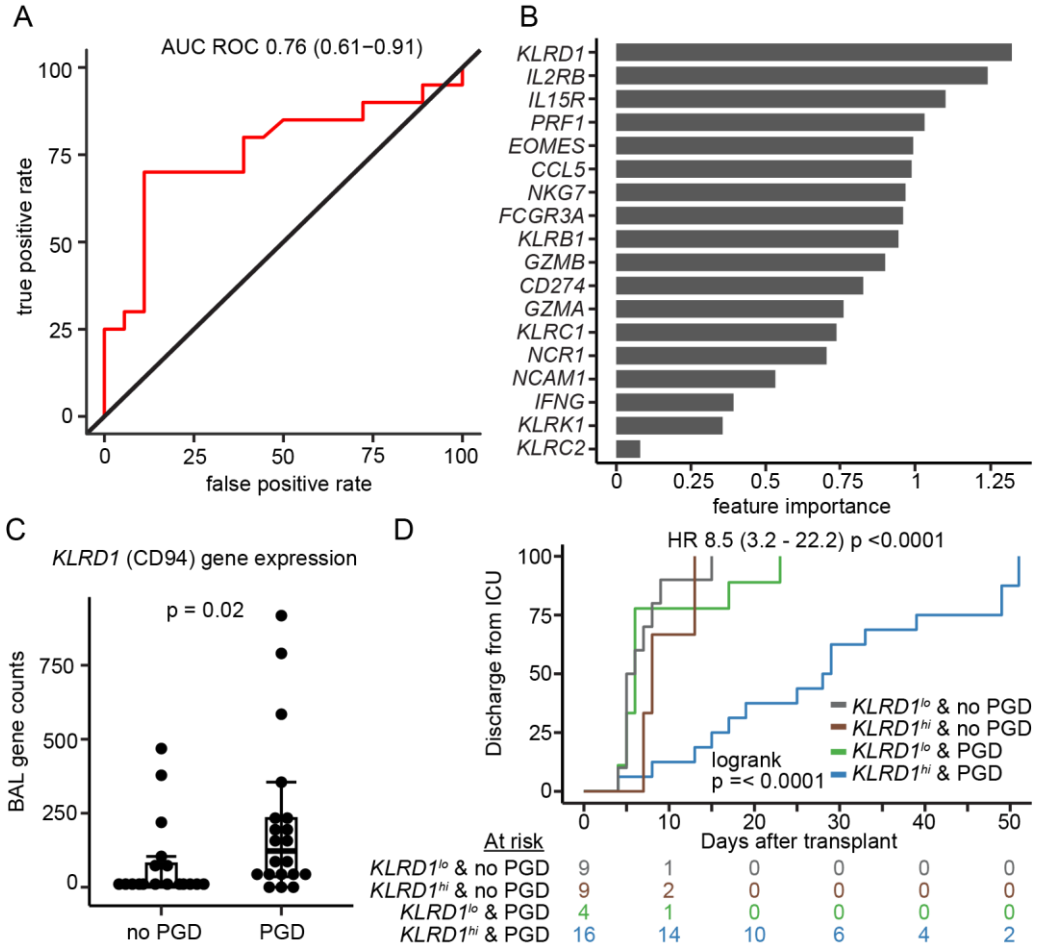

Figure 1. Bronchoalveolar lavage RNA sequencing screen of potential NK cell targets. RNA sequencing was performed on BAL collected on the 1st postoperative day after lung transplantation in recipients with severe PGD (n = 20) and those without PGD (n= 18). We generated a random forest model using 18 NK cell genes as predictors of severe PGD with leave one out validation. (A) Receiver operator curve demonstrating the test characteristics of the model. (B) Relative feature importance of each of the 18 NK cell genes. (C) Transcript counts of *KLRD1*, the top feature in the model, stratified by PGD status. (D) Cumulative incidence plot of discharge from the intensive care unit (ICU) for recipients stratified by high BAL *KLRD1* gene transcript counts and PGD status. Box and whisker plots are bound by 25th and 75th percentile with boxes bisected by the median. Comparisons of gene counts were made with Mann-Whitney U test. Difference in time to ICU discharge was assessed with Cox Proportional Hazards model, displaying log-rank p value.

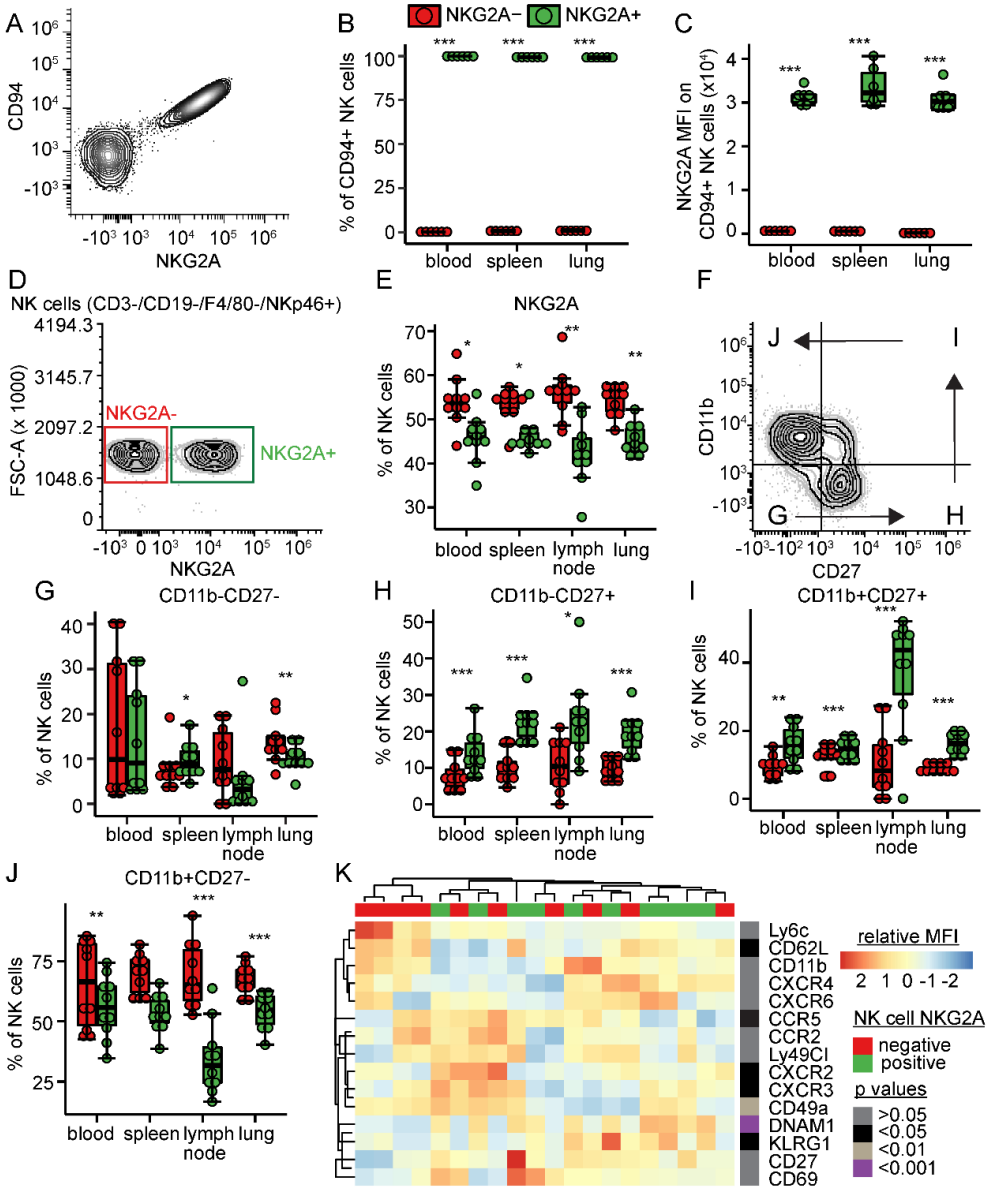

Figure 2. Mouse CD94+ NKG2A+ NK cell profiles. To determine the NK cell expression of CD94 and NKG2A in C57BL/6 mice, several tissues were collected and characterized by spectral flow cytometry. **(A)** NK cells (CD3-CD19-F4/80-NKp46+) expressing CD94 co-express NKG2A in a 1:1 ratio. **(B)** The percentage of NKG2A expression on CD94+ cells is increased across blood, spleen, and lung NK cells. **(C)** In CD94+ NK cells, NKG2A mean fluorescence intensity is increased on CD94+ NK cells **(D)** Representative contour plots of NKG2A gates. **(E)** NKG2A+ NK cells constitute 40-50% of the NK cell population in blood, spleen, lymph node, and lung. **(F)** As indicated by arrow directionality, NK cell maturation is defined by acquisition of CD27, gain of CD11b, and finally loss of CD27 [55]. We assessed differences in NKG2A across the four NK cell maturation states: **(G)**, CD11b-CD27- **(H)** CD11b-CD27+ **(I)**, CD11b+CD27+ and **(J)** CD11b+CD27-. **(K)** We assessed additional activation, chemotaxis, and tissue-resident markers and show differences in MFI in a heatmap. Experiments in B&C studied 5 mice for each condition and other experiments show 10 mice. Box and whisker plots display individual data points bound by boxes at 25th and 75th percentiles and medians depicted with bisecting lines. Differences were assessed using the Mann-Whitney U test with Benjamini-Hochberg corrections for multiple comparisons and paired testing for comparisons within individual animals. P values; * <0.05, ** <0.01, *** <0.001.

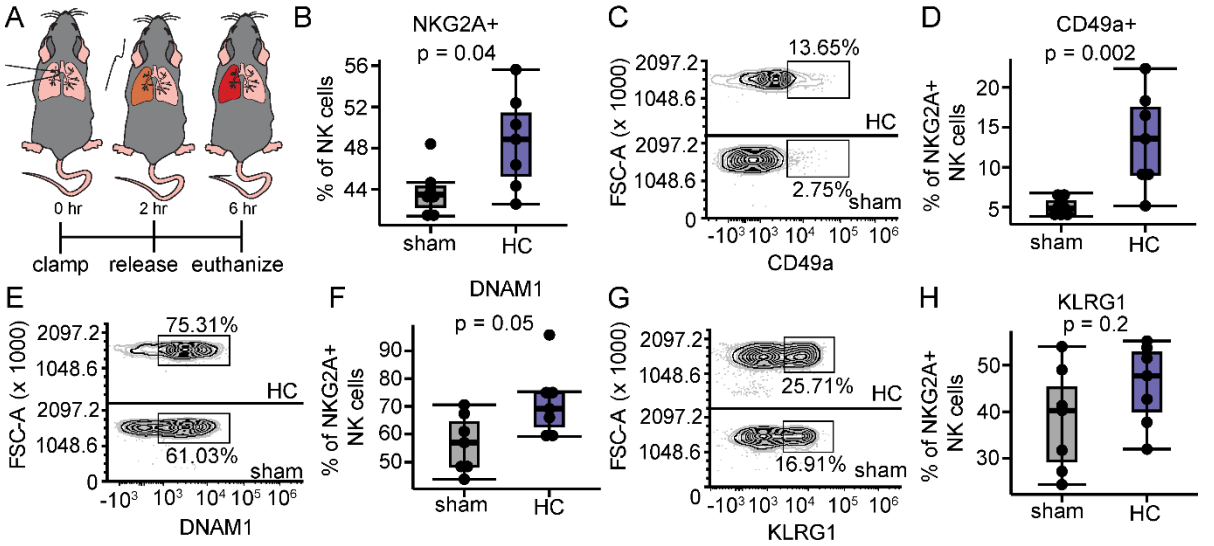

Figure 3. NKG2A+ NK cells in pulmonary ischemia-reperfusion injury. We identified differences during IRI in the NKG2A+ populations. **(A)** We performed warm ischemia reperfusion injury with the hilar clamp model. A slip knot (HC, n = 7) or a sham suture (sham, n = 7) was tied around the left hilum and released 2 hours later, followed by 4 hours of reperfusion before the mice were euthanized. **(B)** There was an increase in percentage of NKG2A+ NK cells in the lungs following hilar clamp. **(C)** Representative contour plots of CD49a in NKG2A+ NK cells. **(D)** CD49a was increased on NKG2A+ NK cells in the lung following HC. **(E)** Representative contour plots of DNAM1 in NKG2A+ NK cells (**F**) Of the NKG2A+ NK cell population, lungs that underwent hilar clamp have an increased percentage of DNAM1. (**G**) Representative contour plots of KLRG1 in NKG2A+ NK cells (**H**) There was no difference in expression of KLRG1 between conditions. Experiments studied 5 mice for each condition. Box and whisker plots display individual data points bound by boxes at 25th and 75th percentiles and medians depicted with bisecting lines. Differences were assessed using the Mann-Whitney U test with $p<0.05$ considered significant.

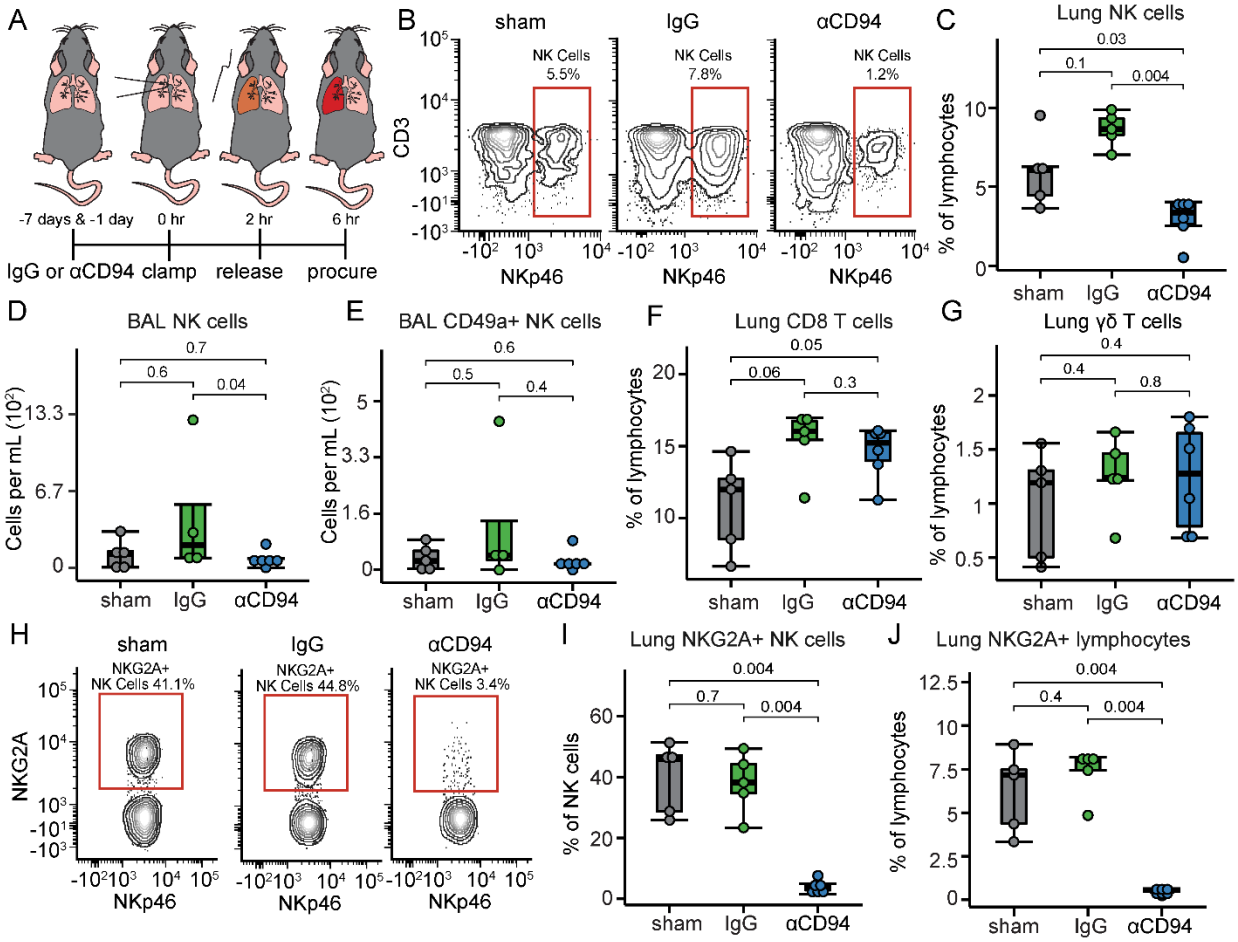

Figure 4. Lung and bronchoalveolar lavage NK cells are reduced with anti-CD94 treatment. (A) C57BL/6 mice underwent sham procedures (n = 5) or were treated with 10 mg/kg of anti-CD94 antibody (n = 6) or isotype-matched control IgG (n = 5) at 7 days and 1 day prior to HC procedures. **(B)** Representative contour plots of NK cells (CD3-CD19-F4/80-NKp46+) across conditions. (**C)** Percentages of lung NK cells were increased during HC in the isotype-matched IgG-treated group and decreased with anti-CD94 treatment. **(D)** Absolute bronchoalveolar lavage NK cells were reduced with anti-CD94 treatment. **(E)** Absolute bronchoalveolar lavage CD49a+ NK cells. **(F)**. CD8+ T cells in the lung across the conditions. (**G**) Percentage of γδ T cells in the lung. (**H**) Representative contour plots of NKG2A+ NK cells in the lung across the 3 conditions. (**I**) Percentage of lung NKG2A+ NK cells. (**J**) Percentage of NKG2A+ lymphocytes in the lung across the conditions. Box and whisker plots display individual data points bound by boxes at 25th and 75th percentiles and medians depicted with bisecting lines. Differences were assessed using the Mann-Whitney U test with Benjamini-Hochberg correction for multiple comparisons with $p<0.05$ considered significant.

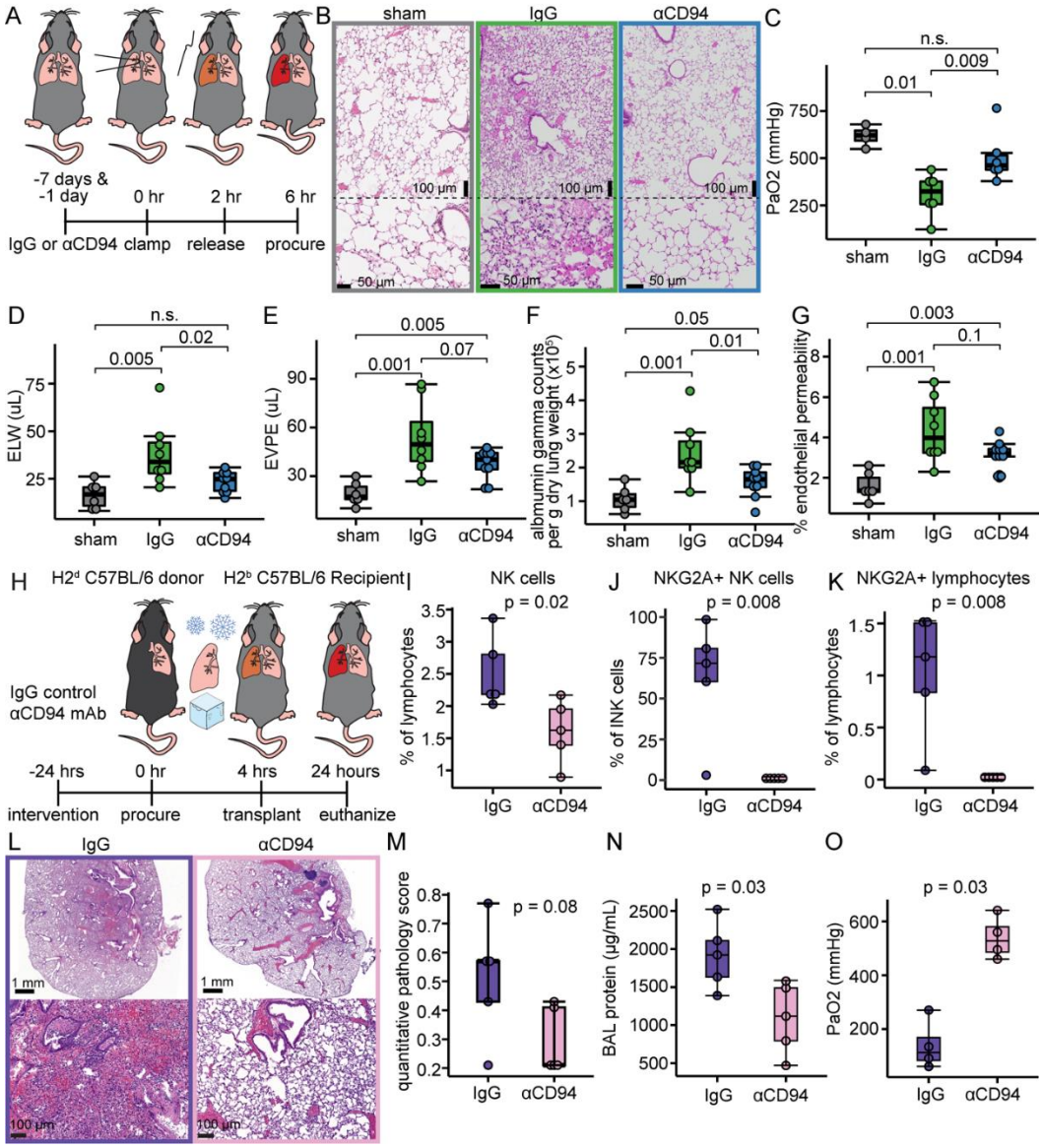

Figure 5. CD94-based NK cell depletion reduces lung ischemia-reperfusion injury. (A) Mice underwent sham procedures or received intraperitoneal anti-CD94 antibody (αCD94**)** or isotype-matched control antibody (IgG) 7 days and 1 day preceding hilar clamp. (**B**) H&E staining of representative lungs (n = 3 per condition). Quantitative injury metrics were collected for each condition and displayed as (**C**) partial pressure of oxygen in arterial blood, (**D**) extravascular lung water, (**E**) extravascular plasma equivalents, (**F**) gamma counts of I^{125}-albumin per gram of dry lung, and (**G**) endothelial permeability. PaO2 experiments show sham-treated (n=5), IgG (n = 6) and anti-CD94-treated mice (n = 6) whereas other metrics display sham-treated (n = 6), IgG (n = 8), and anti-CD94-treated mice (n = 9). (**H)** $H2^d$ C57BL/6 donor and $H2^b$ C56BL/6 recipient mice were treated with intraperitoneal isotype-matched IgG control antibody (IgG, n = 5) or anti-CD94 antibody (αCD94, n = 5) 24 hours preceding the donor lung procurement. $H2^d$ C57BL/6 donor lung was subjected to 4 hours of cold ischemia before orthotopic lung transplant into a C57BL/6 recipient. (**I**) NK cells as a percentage of total lymphocytes in the lung were decreased with treatment. (J) NKG2A+ NK cells in the lung were depleted. (K) NKG2A+ lymphocytes in the lung were depleted. (L) Representative H&E staining of representative lungs (n = 5). We assessed injury via (M) quantitative pathology score, (N) BAL protein, and (O) PaO_2. Box and whisker plots display individual data points bound by boxes at 25^{th} and 75^{th} percentiles and medians depicted with bisecting lines. Differences were assessed using the Mann-Whitney U test with Benjamini-Hochberg correction for multiple comparisons with $p<0.05$ considered significant.

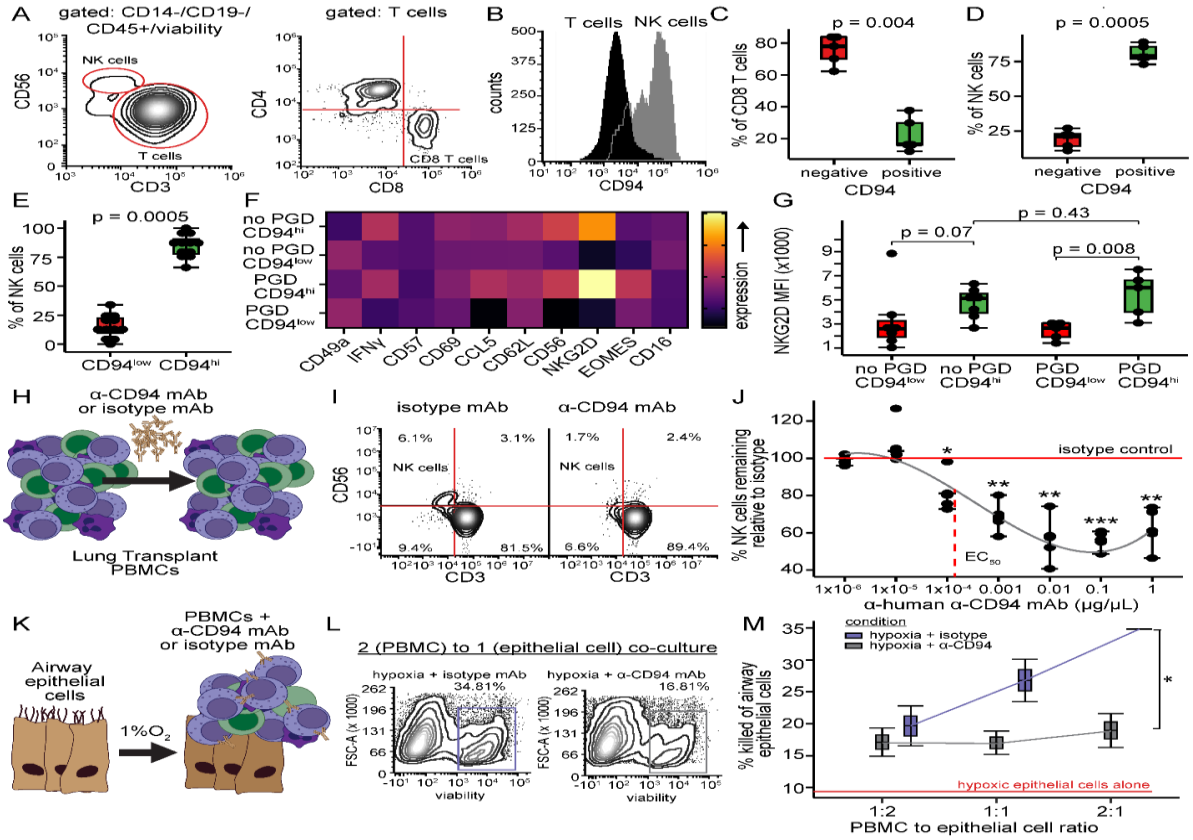

Figure 6. Human lung transplant recipient PBMCs treated with anti-CD94 results in NK cell depletion and reduced *in vitro* IRI. (**A**) NK cells, and CD4 and CD8 T cells were quantified with flow cytometry from lung transplant recipient PBMC (n = 5). CD94 was quantified on PBMCs with plots showing: (**B**) histograms for NK and T cells, (**C**) CD8 T cells, and (**D**) NK cells. NK cell CD94 expression was quantified in BAL from lung transplant recipients with (n = 5) and without PGD (n = 7). (E) NK cells in the BAL have high frequency of CD94 expression. (F) Heatmap of NK cell marker MFI differences between $CD94^{hi}$ and $CD94^{low\ (or\ negative)}$ NK cells from patients with and without PGD. (G) Differences in NKG2D MFI values shown by boxplots. (**H**) *In vitro* depletion of NK cells from lung transplant whole PBMC was performed. (**I**) Representative contour plots from isotype-matched control IgG-treated and anti-CD94 (αCD94)-treated PBMCs treated at 0.1ug/ul. (**J**) Percentages of NK cells are shown relative to IgG control across different anti-CD94 concentrations (**K**) To assess cytotoxicity, airway epithelial cells were subjected to hypoxia (1% O_2) for 24 hours and then co-cultured with PBMCs treated with control IgG or anti-CD94 antibody for an additional 24 hours. Airway epithelial cells are stained with CellTrace Violet prior to plating to distinguish PBMCs from epithelial cells during flow cytometry analysis. (**L**) Representative contour plots of viability in co-culture across 2 conditions at 2:1 PBMC to epithelial ratio. (**M**) Killing plots of airway epithelial cells across the 2 conditions. Box and whisker plots display individual data points bound by boxes at 25^{th} and 75^{th} percentiles and medians depicted with bisecting lines. Differences were assessed using the Mann-Whitney U test. P values; * p<0.05, ** p <0.01, and *** p <0.001.

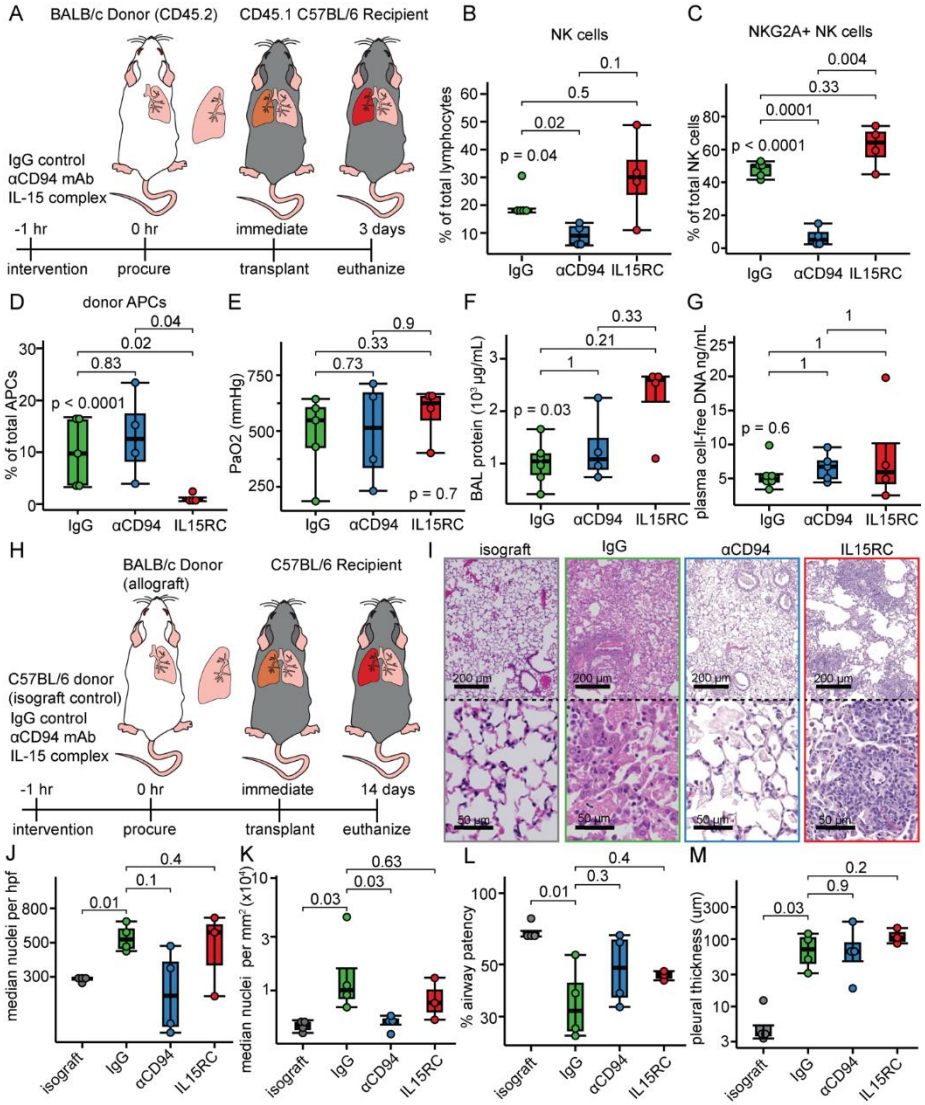

Figure 7. CD94-based NK cell depletion in the allogeneic orthotopic lung transplant model (A) CD45.1 C57BL/6 mice were treated with intraperitoneal isotype-matched IgG control antibody (IgG, n = 5), anti-CD94 antibody (αCD94, n = 4), or IL-15-IL-15 receptor complex (IL15RC, n = 4) 1-hour preceding orthotopic lung transplant with minimal warm ischemia from a BALB/c donor. We measured lung allograft (**B**) total NK cells, (**C**) NKG2A+ NK cells, (**D**) donor APCs. Injury was quantified by (**E**) PaO_2, (**F**) BAL protein, and (**G**) plasma cell-free DNA. (**H**) We also assessed chronic injury on post-operative day 14 in isografts (n = 4) and allograft recipients pre-treated with intraperitoneal isotype-matched IgG control antibody (IgG, n = 4), anti-CD94 antibody (αCD94, n = 4), or IL-15-IL-15 receptor complex (IL15RC, n = 3) 1-hour preceding orthotopic lung transplant with minimal warm ischemia from a BALB/c donor. (**I)** Representative H&E slide sections from each group. We assessed pathologic injury via (**J)** median nuclei per high powered field (hpf), (**K**) median nuclei surrounding the airways per square millimeter, (**L**) airway patency, and (**M**) pleural thickness. Box and whisker plots display individual data points bound by boxes at 25th and 75th percentiles and medians depicted with bisecting lines. Comparisons across experimental groups were made with the Kruskal Wallis test. Differences were assessed using the Mann-Whitney U test with Benjamini-Hochberg correction for multiple comparisons with $p<0.05$ considered significant.

SUPPLEMENTAL MATERIAL
Supplemental Tables
Supplemental Table 1. Human BAL immunophenotyping cohort characteristics

	No PGD (N = 7)	PGD (N = 5)	P value
Age, mean (SD)	60.7 (8.1)	55.2 (13.1)	0.44
Female sex, N (%)	4 (47.1)	1 (20)	0.49
Diagnosis group, N (%)			1
COPD	1 (14.3)	1 (20)	
ILD	6 (85.7)	4 (80)	
Double transplant, N (%)	7 (100)	5 (100)	1
Ethnicity, N (%)			0.83
Caucasian	3 (42.9)	2 (40)	
Hispanic	1 (14.3)	0 (0)	
Asian	2 (28.6)	2 (40)	
Multiracial	1 (14.3)	1 (20)	

Supplemental Table 2. Markers for CD94+ NK cell spectral cytometry panel				
Fluorophore	Marker	Clone	Supplier	Catalog #
BUV395	CD25	PC61	BD Biosciences	564022
BUV615	CD11c	N418	BD Biosciences	751222
Viability UV	Live/Dead Blue	NA	ThermoFisher Scientific	L34962
BUV661	CD11b	M1/70	BD Biosciences	612977
BUV737	CD49a	Ha31/8	BD Biosciences	741776
BV421	KLRG1	2F1/KLRG1	BioLegend	138414
Pacific Blue	CD69	H1.2F3	BioLegend	104524
BV510	PD1	29F.1A12	BioLegend	135241
BV570	Ly6C	HK1.4	BioLegend	128030
BV605	NK1.1	PK136	BioLegend	108740
BV650	Ly49C/I	5E6	BD Biosciences	744030
BV711	NKp46	29A1.4	BioLegend	137621
FITC	CD94	18d3	ThermoFisher Scientific	11-0941-82
Perc	CD8a	53-6.7	BioLegend	100732
Perc/Cy5.5	CD45.2	104	BioLegend	109828
Perc-eFluor 710	NKG2D	CX5	ThermoFisher Scientific	46-5882-82
PE	NKG2AB6	16A11	ThermoFisher Scientific	12-5897-83
PE/Dazzle594	CD27	LG.3A10	BioLegend	124228
PE/Cy5	CD62L	MEL-14	BioLegend	104410
PE/Cy7	CD49b	HMα2	BioLegend	103518
APC	CD16	S17014E	BioLegend	158006
APC-Cy7	CD3	17A2	BioLegend	100222
Alexa Fluor 700	CD19	6D5	BioLegend	115528

Supplemental Table 3. Mouse spectral flow cytometry antibodies in IRI

Fluorophore	Marker	Clone	Supplier	Catalog #
BUV395	CD27	LG 3A10	BD Biosciences	740247
Viability UV	Live/Dead	N/A	Invitrogen	L34962
BUV496	CXCR2	V48-2310	BD Biosciences	750142
BUV563	CXCR3	CXCR3-173	BD Biosciences	741438
BUV615	CCR2	475301	BD Biosciences	751074
BUV737	CCR3	83103	BD Biosciences	741699
BUV805	NKG2ACE	20D5	BD Biosciences	741990
BV421	NKp46	29A1.4	BioLegend	137612
SB436	NK1.1	PK136	ThermoFisher	62-5941-82
Pacific Blue	CD69	H1.2F3	BioLegend	104524
BV510	CD19	6D5	BioLegend	115545
Pacific Orange	CD8a	5H10	ThermoFisher	MCD0830
BV570	Ly6C	HK1.4	BioLegend	128030
BV605	Ly49C/I	5E6	BD Biosciences	744029
BV650	CD11b	M1/70	BioLegend	101239
BV711	DNAM1	TX42.1	BioLegend	133609
BV785	KLRG1	2F1/KLRG1	BioLegend	138429
BB515	CCR5	C34-3448	BD Biosciences	565093
Spark Blue 550	CD3e	17A2	BioLegend	100259
PerCP	CD45	30-F11	BioLegend	103130
BB700	CD49a	Ha31/8	BioLegend	742164
PerCP/Cy5.5	CCR4	2G12	BioLegend	131220
PE	S1P5	1196A	R&D	FAB9084P
PE/Dazzle594	CX3CR1	SA011F11	BioLegend	149014
AlexaFluor594	MHC-II	M5/114.15.2	BioLegend	107650
PE/Cy5	gdTCR	GL3	ThermoFisher	15-5711-81
PE/Cy5.5	CXCR4	2B11	ThermoFisher	35-9991-80
PE/Cy7	CD49b	DX5	BioLegend	108921
APC	CCR1	S15040E	BioLegend	152504
AlexaFluor647	CXCR6	SA051D1	BioLegend	151115
APC-R700	F4/80	T45-2342	BD Biosciences	565787
APC/eF780	CD62L	MEL-14	ThermoFisher	47-0621-80

Supplemental Table 4. Antibodies for mouse immunophenotyping

Fluorophore	Marker	Clone	Supplier	Catalog #
Fixable Viability Blue	Live/Dead	N/A	Invitrogen	L23105
AF700	CD45	30-F11	BD Biosciences	560510
PerCP	CD3e	145-2C11	BioLegend	553067
PE	NKG2A	16A11	BioLegend	142804
FITC	NKp46	29A1.4	BD Biosciences	560756
BV605	CD19	1D3	BD Biosciences	563148
BV421	F4/80	T45-2342	BD Biosciences	565411
APC	CD49a	HMα1	BioLegend	142606
APC/Fire750	CD8a	53-6.7	BioLegend	100766
PE/Cy7	γδTCR	GL3	BioLegend	118124

Supplemental Table 5. Donor antigen presenting cell cytometry panel

Fluorophore	Marker	Clone	Supplier	Catalog #
Fixable Viability Blue	Live/Dead	N/A	Invitrogen	L23105
BV421	F4/80	T45-2342	BD Biosciences	545411
PerCP	CD3e	145-2C11	BD Biosciences	145-2C11
FITC	NKp46	29A1.4	BioLegend	560756
PE	NKG2A	16A11	BioLegend	142804
APC	CD45.1	A20	BioLegend	110713
APC/Fire750	CD45.2	104	BioLegend	109851
PE/Cy7	CD11c	N418	BioLegend	117317

Supplemental Table 6. Baseline characteristics for human depletion

Patient	Age	Sex	Transplant type	Race or Ethnicity	Diagnosis
A	70	M	Single	Caucasian	COPD
B	69	M	Double	Caucasian	COPD
C	60	F	Double	Caucasian	COPD
D	60	M	Double	Hispanic	COPD
E	56	F	Double	Asian	COPD

Supplemental Table 7. Human quantification antibodies

Fluorophore	Marker	Clone	Supplier	Catalog #
BUV395	CD45	HI30	BD Bioscience	563792
BV605	CD3	SK7	BioLegend	344836
PerCP-Cy5.5	CD4	OKT4	BioLegend	317428
BV786	CD8	SK1	BioLegend	344740
APC/Cy7	CD19	HIB19	BioLegend	302218
PE/Cy7	CD14	M5E2	BioLegend	301814
FITC	CD56	HCD56	BioLegend	318304
BV510	CD57	3G8	BioLegend	302026
AF700	CD16	QA17A04	BioLegend	393314
APC	CD94	HP-3D9	BD Bioscience	559876
PE	NKG2A	Z199	Beckman Coulter	IM3291U
BV421	NKG2D	1D11	BioLegend	320822
PE-CF594	viability		BioLegend	77475

Supplemental Table 8. Human BAL RNA sequencing cohort baseline characteristics

Variable	No PGD (N = 18)	Severe PGD (N = 20)	P value
Age, mean (SD)	61.9 (9.4)	55.3 (15.7)	0.12
Male Sex, N (%)	10 (55.6)	6 (30)	0.21
Diagnosis, N (%)			0.94
COPD	3 (16.7)	2 (10)	
PAH	1 (5.6)	1 (5)	
CF	1 (5.6)	1 (5)	
ILD	13 (72.2)	16 (80)	
Transplant Type, N (%)			1
Single-Lung	0 (0)	1 (5)	
Double-Lung	18 (100)	19 (95)	
Ethnicity, N (%)			0.82
Caucasian	14 (77.8)	14 (70)	
African American	1 (5.6)	1 (5)	
Hispanic	3 (16.7)	5 (25)	

Supplemental Figures

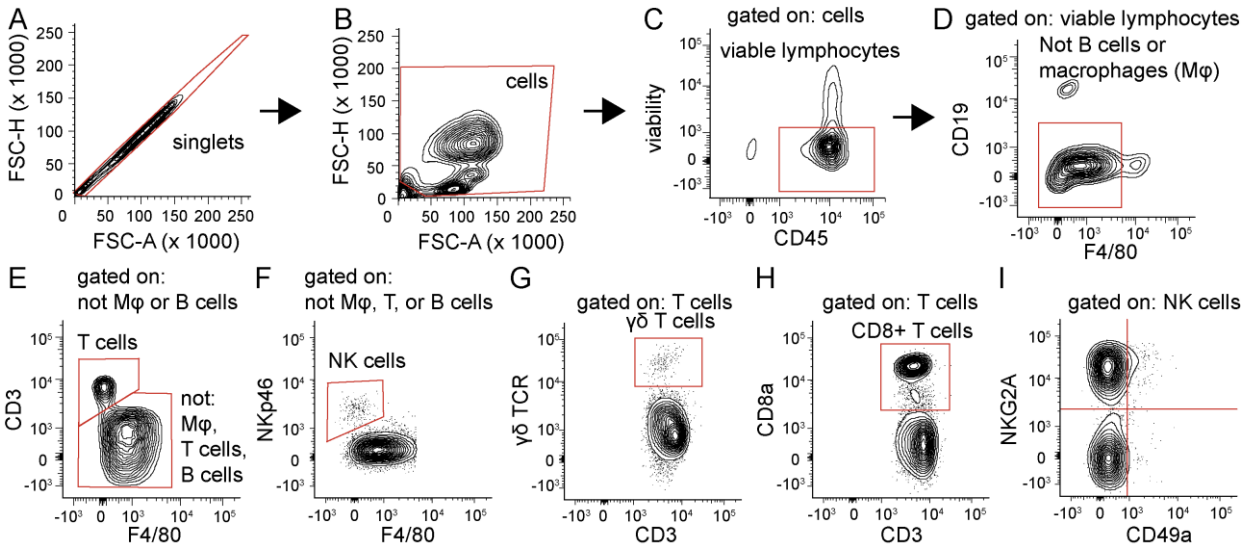

Supplemental Figure 1. NK cell and T cell gating strategy. Events were gated by: **(A)** Single cells**, (B)** cells, **(C)** viable lymphocytes, **(D)** cell lacking B cell or macrophage markers, **(E)** presence of CD3, **(F)** NK cells**, (G)** γδ T cells, **(H**) CD8 T cells, and by expression of **(I)** NKG2A.

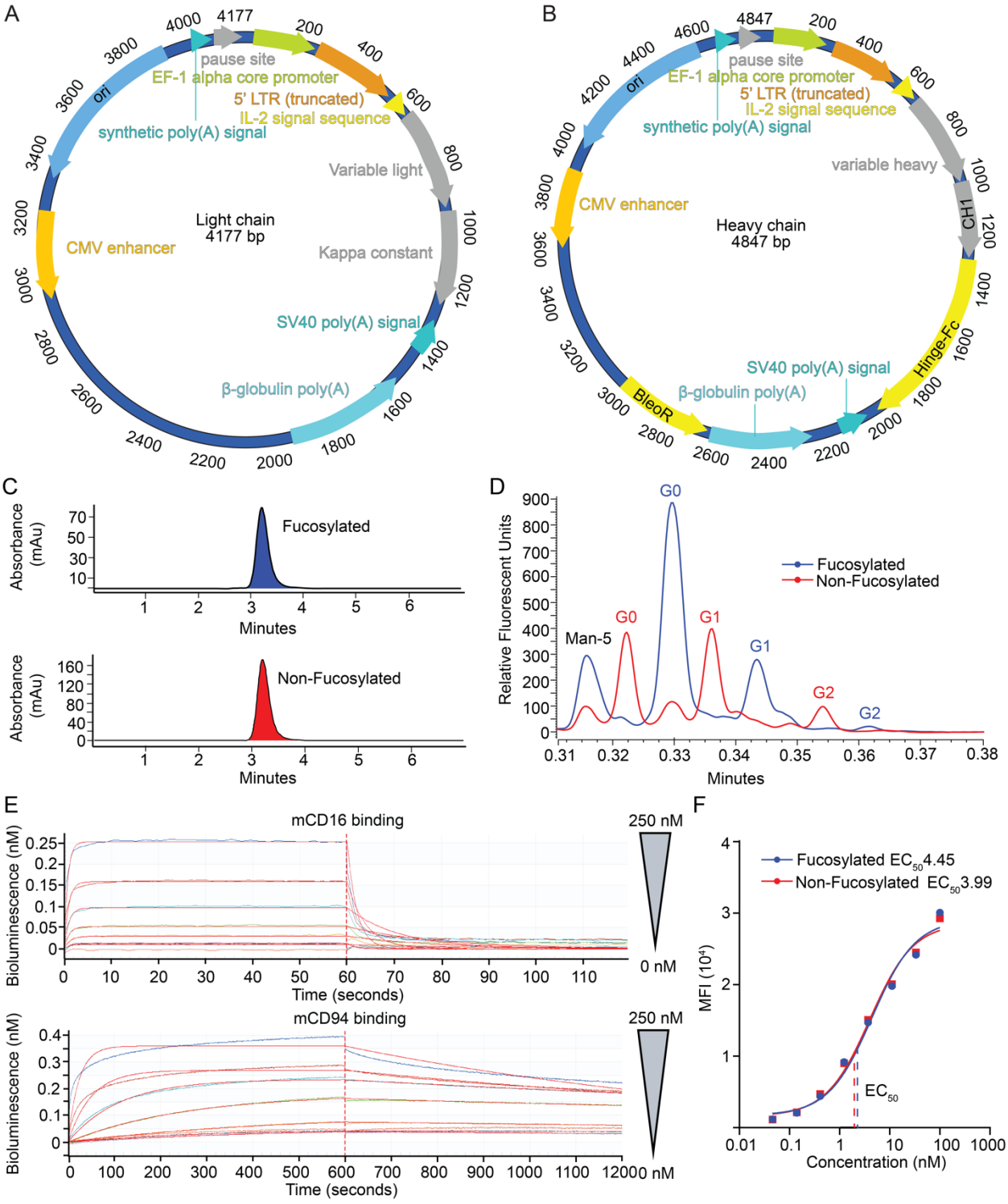

Supplemental Figure 2. Anti-mouse anti-CD94 monoclonal antibody characteristics. (A) Plasmid map for construction of the mAb light chain. Anti-CD94 variable light region was cloned into a plasmid expressing the mouse kappa chain constant region. (**B**) Plasmid map for construction of the mAb heavy chain. Anti-CD94 variable heavy region was cloned into a plasmid expressing the mouse IgG1 heavy chain. **(C)** Fucosylated and non-fucosylated antibodies were purified by size exclusion chromatography. **(D)** Glycan distribution across fucosylated and non-fucosylated antibodies**. (E)** Binding of anti-mouse anti-CD94 monoclonal antibody to mouse CD16 (mCD16) compared to mouse CD94 (mCD94**). (F)** Anti-mouse anti-CD94 monoclonal antibody affinity for CD94+ Ba/F3 cells across a range of concentrations.

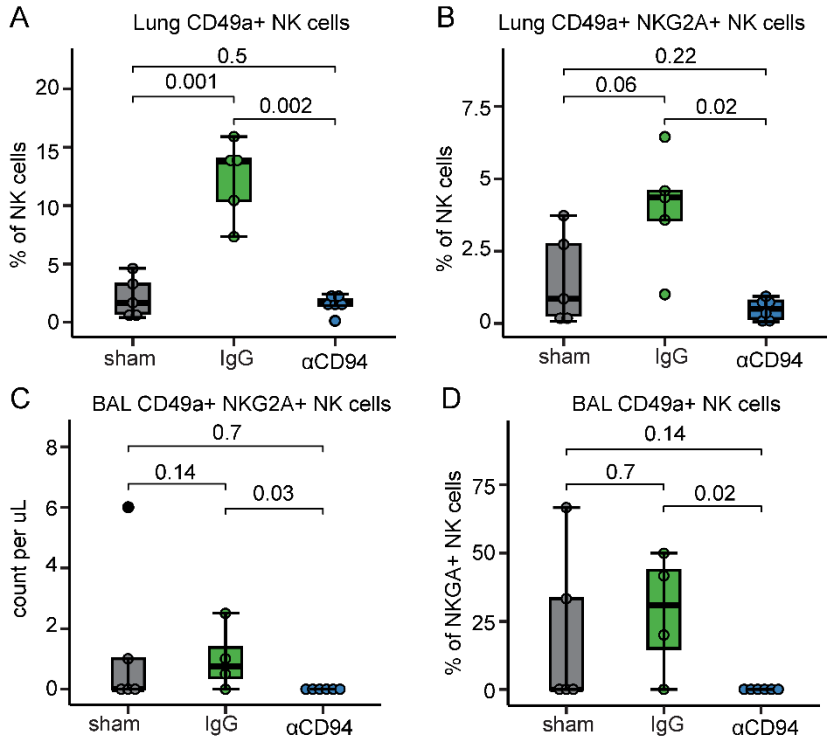

Supplemental Figure 3. Lung and BAL NK cell expression of CD49a and NKG2A in the HC IRI model. (A) Lung CD49a+ NK cells as a percentage of the total NK cell population across HC and sham conditions. **(B)** Percent of lung CD49a+NKG2A+ NK cells. **(C)** Absolute count of BAL CD49a+NKG2A+ NK cells. **(D)** Percent of BAL NKG2A+ NK cells that are CD49a+.

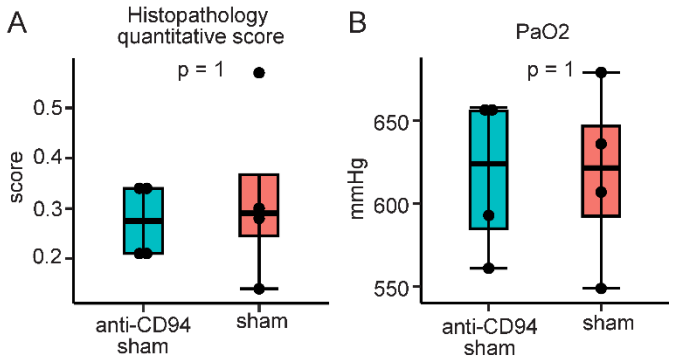

Supplemental Figure 4. Comparisons across shams. (A) Histopathology scores and (B) arterial PaO2 were compared between sham animals that received anti-CD94 monoclonal antibody 24 hours preceding sham thoracotomy and sham animals with no treatment. Differences were assessed via Mann Whitney U testing.

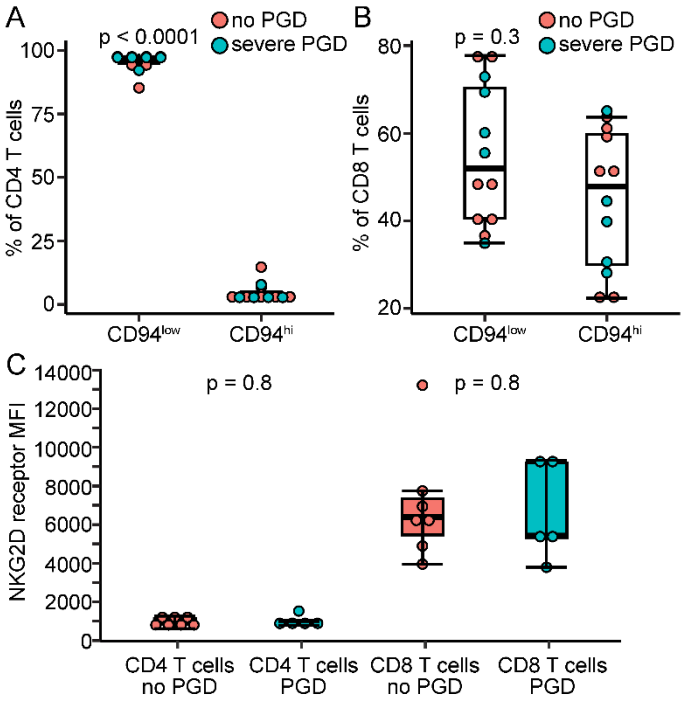

Supplemental Figure 5. BAL T cell characteristics of patients with and without PGD. (A) CD94 expression as a percentage of CD4 T cells. (B) CD94 expression as a percentage of CD8 T cells. (C) NKG2D MFI on CD4 and CD8 T cells in patients with and without PGD.

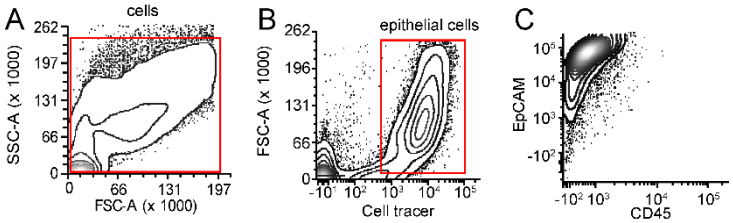

Supplemental Figure 6. Coculture Killing Assay Gating Strategy for Epithelial Cells. CellTrace-labeled epithelial cells were gated by **(A)** size and **(B)** CellTrace expression. **(C)** EpCAM expression was used to confirm CellTrace labeling of epithelial cells.

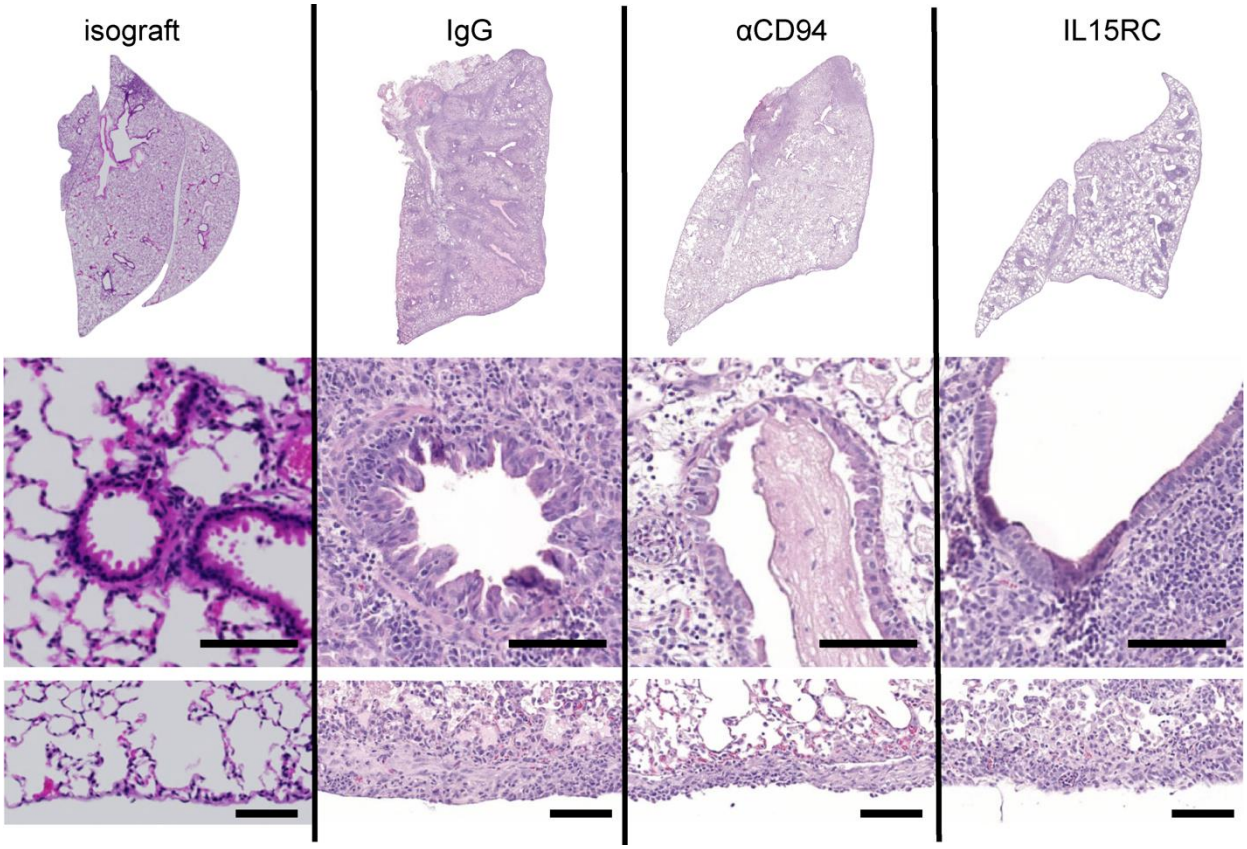

Supplemental Figure 7. 14-day pathology from OLT models. The top row shows low magnification representative lung sections with H&E staining. The middle row shows representative airways from each condition. The bottom row displays representative pleura from each condition. Bars represent 100 um.

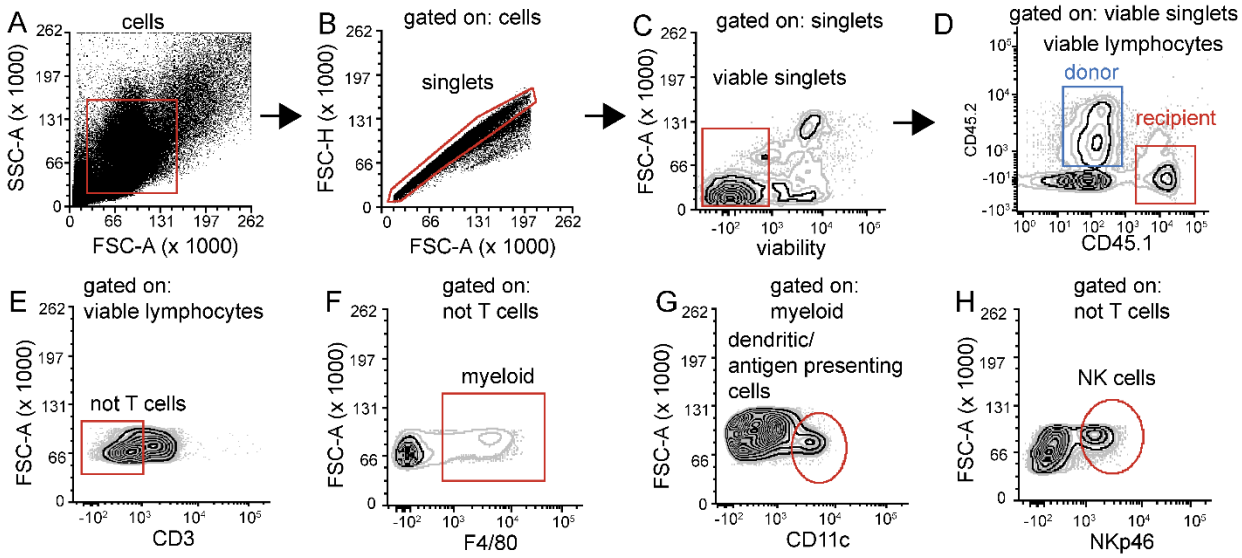

Supplemental Figure 8. Donor antigen presenting cell (APC) gating strategy. Events were gated to define **(A)** cells**, (B)** singlets, **(C)** viable cells, **(D)** lymphocyte of donor or recipient origin, **(E)** T cells**, (F)** myeloid cells, (**G**) APCs and (**H**) NK cells.

anti-CD94 monoclonal antibodies target mouse and human NK cells for depletion

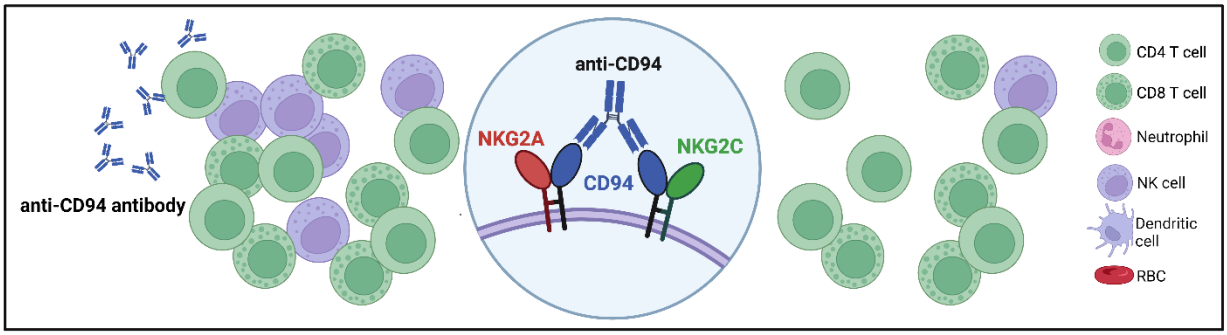

Lung ischemia-reperfusion injury